

1 **Short title:** CARP9 and HYL1 interact to promote AGO1 stability

2

3 **Title: The intrinsically disordered protein CARP9 bridges HYL1 to AGO1 in the nucleus**
4 **to promote micro RNA activity**

5 Ariel H. Tomassi^{1,2}, Delfina A. Re^{1,2}, Facundo Romani¹, Damian A. Cambiagno¹, Lucía
6 Gonzalo¹, Javier E. Moreno¹, Agustin L. Arce¹, Pablo A. Manavella^{1,*}

7

8 ¹Instituto de Agrobiotecnología del Litoral (CONICET-UNL-FBCB), 3000, Santa Fe, Argentina

9 ²Both authors contributed equally

10 *To whom correspondence should be addressed. E-mail pablomanavella@ial.santafe-
11 conicet.gov.ar

12

13 **One-sentence summary**

14 An intrinsically disordered protein__interacts with HYPONASTIC LEAVES1 and
15 ARGONAUTE1 in a post-miRNA processing complex to promote ARGONAUTE1 stability
16 and miRNA activity.

17

18 **Author contributions:** AHT, DAR and PAM conceived the research. AHT, DAR, DAC and LG
19 carried out the experimental work. ALA analyzed sequencing data. FR and JEM performed the
20 evolutionary and conservation analysis. AHT, DAR, PAM interpreted results and wrote the paper. All
21 authors read, edited, and approved the final version of the manuscript.

22

23 **ABSTRACT**

24 In plants, small RNAs (sRNA) are loaded into ARGONAUTE (AGO) proteins to fulfill their
25 regulatory functions. Micro RNAs (miRNAs), one of the most abundant classes of endogenous
26 sRNAs, are preferentially loaded into ARGONAUTE1 (AGO1). Such loading, long believed to
27 happen exclusively in the cytoplasm, was recently proposed to also occur in the nucleus. Here
28 we identified CONSTITUTIVE ALTERRATIONS IN THE SMALL RNAS PATHWAYS9
29 (CARP9), a nuclear-localized, intrinsically disordered protein, as a factor promoting miRNA
30 activity in Arabidopsis (*Arabidopsis thaliana*). Mutations in the CARP9-encoding gene led to a
31 mild reduction of miRNAs levels, impaired gene silencing, and characteristic morphological
32 defects, including young leaf serration and altered flowering time. Intriguingly, we found that
33 CARP9 was able to interact with HYPONASTIC LEAVES1 (HYL1), but not with other
34 proteins of the miRNA biogenesis machinery. In the same way, CARP9 appeared to interact
35 with mature miRNA, but not with pri-miRNA, positioning it after miRNA processing in the
36 miRNA pathway. CARP9 was also able to interact with AGO1, promoting its interaction with
37 HYL1 to facilitate miRNA loading in AGO1. Plants deficient in CARP9 displayed reduced

38 levels of AGO1-loaded miRNAs, partial retention of miRNA in the nucleus, and reduced levels
39 of AGO1. Collectively, our data suggest that CARP9 might modulate HYL1AGO1 crosstalk,
40 acting as a scaffold for the formation of a nuclear post pri-miRNA processing complex that
41 includes at least HYL1, AGO1 and HSP90. In such a complex, CARP9 stabilizes AGO1 and
42 mature miRNAs, allowing the proper loading of miRNAs in the effector complex.

43

44 INTRODUCTION

45 Post-transcriptional regulation of gene expression mediated by miRNAs controls numerous
46 processes during plant development and response to the environment (Li et al., 2017). In
47 *Arabidopsis* (*Arabidopsis thaliana*), RNA polymerase II transcribes *MIRNA* loci to primary
48 miRNAs (pri-miRNAs), which are processed into mature ~21 nt miRNA duplexes by multiple
49 and sequential cuts (Bologna et al., 2013; Zhu et al., 2013; Moro et al., 2018). The RNase-III
50 endonuclease DICER-LIKE 1 (DCL1), together with the RNA binding protein HYPONASTIC
51 LEAVES 1 (HYL1) and the zinc finger protein SERRATE (SE), recognizes and processes pri-
52 miRNAs into mature miRNA duplexes (Kurihara and Watanabe, 2004; Dong et al., 2008). In
53 addition, numerous accessory proteins were identified lately to regulate the miRNA biogenesis
54 at different stages (Rogers and Chen, 2012; Achkar et al., 2016; Manavella et al., 2019). HYL1
55 was proposed to remain bound to the mature miRNA duplexes and interact with HUA
56 ENHANCER 1 (HEN1), acting as a scaffold to ensure miRNA methylation (Li et al., 2005;
57 Yang et al., 2010; Baranauske et al., 2015). Mature miRNAs, potentially still bound by to
58 HYL1, are then loaded into an AGO protein, with AGO1 as the main effector of the miRNA
59 pathway in plants, to fulfill their functions (Fang and Qi, 2016). Loading of miRNA duplexes
60 into AGO1 and the assembly of the RNA-Induced Silencing Complex (RISC) were initially
61 thought to be cytoplasmic exclusive processes (Bologna and Voinnet, 2014). This was inferred
62 from metazoan cells where miRNA loading into the RISC occurs in the cytosol, and the fact that
63 the homolog of the human EXPORTIN-5 of *Arabidopsis*, known as HASTY (HST), showed
64 impaired miRNA accumulation (Park et al., 2005). A recent report demonstrated that AGO1 is
65 at least partially loaded with miRNA duplexes in the nucleus and then exported to the cytosol as
66 an AGO1:miRNA complex (Bologna et al., 2018). It is not clear if the nuclear AGO1 loading is
67 dependent on HYL1. However, some evidences suggested that this is a certain possibility: 1)
68 AGO1 colocalizes with HYL1 in nuclear speckles (Fang and Spector, 2007); 2) HYL1 is
69 required for the proper miRNA loading and strand selection by AGO1 (Eamens et al., 2009;
70 Manavella et al., 2012); and 3) HYL1 remains bound to mature miRNAs after processing (Yang
71 et al., 2010). ENHANCED MIRNA ACTIVITY1 (EMA1) and TRANSPORTIN1 (TRN1) were
72 also shown to interact with AGO1 and modulate miRNAs loading into AGO1 (Wang et al.,
73 2011; Cui et al., 2016). The finding of the nuclear loading of AGO1 not only created a new

74 model for miRNAs export but also rationalized the recently identified nuclear functions of
75 AGO1 (Dolata et al., 2016; Schalk et al., 2017; Liu et al., 2018).

76 Using a forward genetic screening, we identified CONSTITUTIVE ALTERATIONS IN
77 THE SMALL RNAS PATHWAYS 9 (CARP9), a predicted intrinsically disordered protein
78 (IDP), as a new partner of the miRNA pathway. Mutations in *CARP9* produced morphological
79 alterations, a mild reduction in the miRNA accumulation, and impaired gene silencing. We
80 found that CARP9 interacts with HYL1 in discrete nuclear speckles promoting HYL1-AGO1
81 interaction. Our data suggest that CARP9 did not participate in pri-miRNAs processing, but
82 instead it is associated with HYL1 and mature miRNAs in a post-miRNA-processing complex.
83 In such complex, we found that CARP9 also interacts with AGO1 and HEAT SHOCK
84 PROTEIN 90 (HSP90). *CARP9* mutants presented low levels of AGO1-associated miRNAs, a
85 reduction of AGO1 levels, and an apparent depletion of miRNAs in the cytoplasm. All this
86 evidence allow us to suggest that CARP9 could be acting as a scaffold protein, connecting
87 HYL1 to AGO1 in a post pri-miRNAs processing complex, ensuring AGO1 stability thus
88 leading to the proper loading of the AGO1:miRNA complexes, likely before its export to the
89 cytosol.

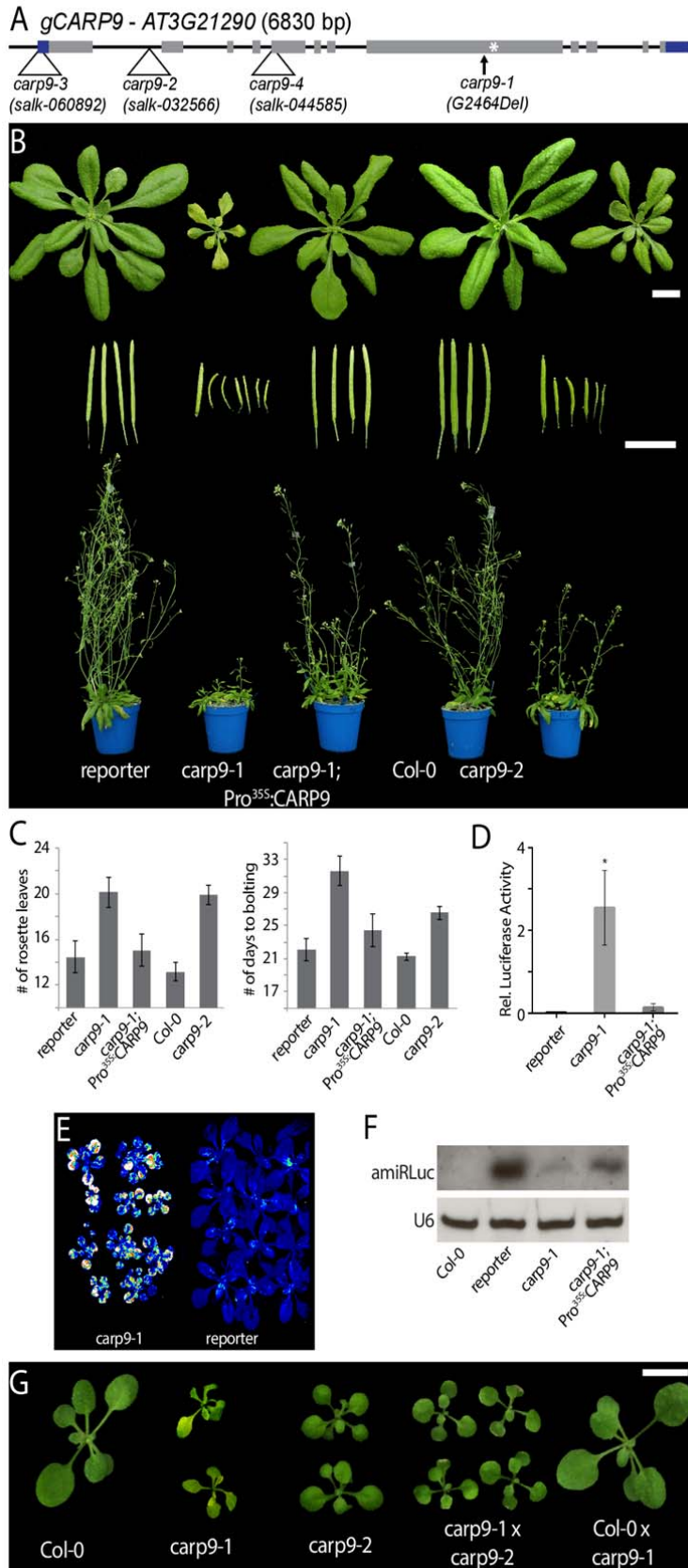
90

91

92 **RESULTS**

93 **Identification of CARP9 from a miRNA-activity screen**

94 During the last years, we characterized several miRNA deficient mutants isolated from a genetic
95 screening based on the silencing of a luciferase reporter by an artificial miRNA (amiRLUC)
96 (Manavella et al., 2012; Francisco-Mangilet et al., 2015; Karlsson et al., 2015; Re et al., 2020).
97 Here, using mapping by sequencing (Sun and Schneeberger, 2015), we localized the causal
98 mutation in one of the isolated plants, named *constitutive alterations in the small RNAs*
99 *pathways 9 (CARP9)*, to a small region of chromosome 3 (Supplemental Figure S1A). Within
100 this region, we detected a single nucleotide deletion (G2464Del, *AT3G21290*, Chr3:7486786,
101 TAIR10) resulting in a premature stop codon and an aberrant C-terminal region of 34 amino
102 acids (Figure 1A). Compared to the reporter plants, this mutant allele (named *carp9-1*) showed a
103 reduced stature, irregular young leaves edges, pale green color, shorter and twisted siliques, a
104 delay in flowering time, and observable defects in the architecture of flowers, including shorter
105 stamens (Figure 1B, 1C, and Supplemental Figure S1B and S1C). Transformation of the mutant
106 with a WT copy of *CARP9* cDNA, either expressed under the 35S promoter or its native
107 regulatory region, fully reverted the morphological phenotype of the mutant (Figure 1B, 1C, and
108 Supplemental Figure S1B and S1C). In the overexpressing lines, we selected lines with low
109 expression levels for the analyses. Besides, the *carp9-1* mutant showed elevated luciferase
110 activity with a severe reduction of the amiRLUC levels (Figure 1D, 1E and 1F). All
111 morphological defects of *carp9-1* were also observed, to a lesser degree, in a mutant with a T-
112 DNA insertion within the first intron of this gene named *carp9-2* (Figure 1A, 1B, 1C, and
113 Supplemental Figure S1B). To further confirm that the mutation in *AT3G21290* was causing the
114 observed phenotype, we crossed *carp9-1* and *carp9-2* mutants and analyzed the progeny. The
115 compound heterozygotes offspring showed similar phenotypes to the parental lines confirming
116 that the mutation in *CARP9* was the cause of the observed phenotypes (Figure 1G). In the case
117 of a third allele, *carp9-3* (*SALK_060892*), bearing a T-DNA insertion in the 5'-UTR region of
118 *CARP9* approximately 100 bp upstream the ATG codon (Figure 1A), we were not able to
119 recover any homozygous line suggesting that plants are not viable when this mutation is
120 homozygous. Interestingly, we did not find signs of embryonic abortion or impaired
121 germination/growth in *carp9-3 +/-* progeny (Supplemental Figure S1D and S1E). Nevertheless,
122 all genotyped seedlings were either WT or heterozygous for *carp9-3* mutation suggesting a
123 problem with the male gametes. Supporting this scenario, we were not able to detect the *carp9-3*
124 insertion in the offspring of WT plants fertilized with pollen of *carp9-3* heterozygous plants.
125 Similarly, we failed to detect the homozygous insertion in the *SALK_044585* allele (*carp9-4*),
126 which is annotated to have an insertion in *CARP9* fifth exon (Figure 1A). Altogether, the
127 analysis of these alleles suggests that *CARP9* is essential for the plant development and points
128 *carp9-1* and *carp9-2* as hypomorphic alleles. In this sense, *carp9-1* may still produce a



129 truncated but active protein, while *carp9-2* partially reduces CARP9 transcription as indicated

130 by RT-qPCR analysis (Supplemental Figure S1F).

131

132 **CARP9 displayed impaired activity of the miRNA pathway**

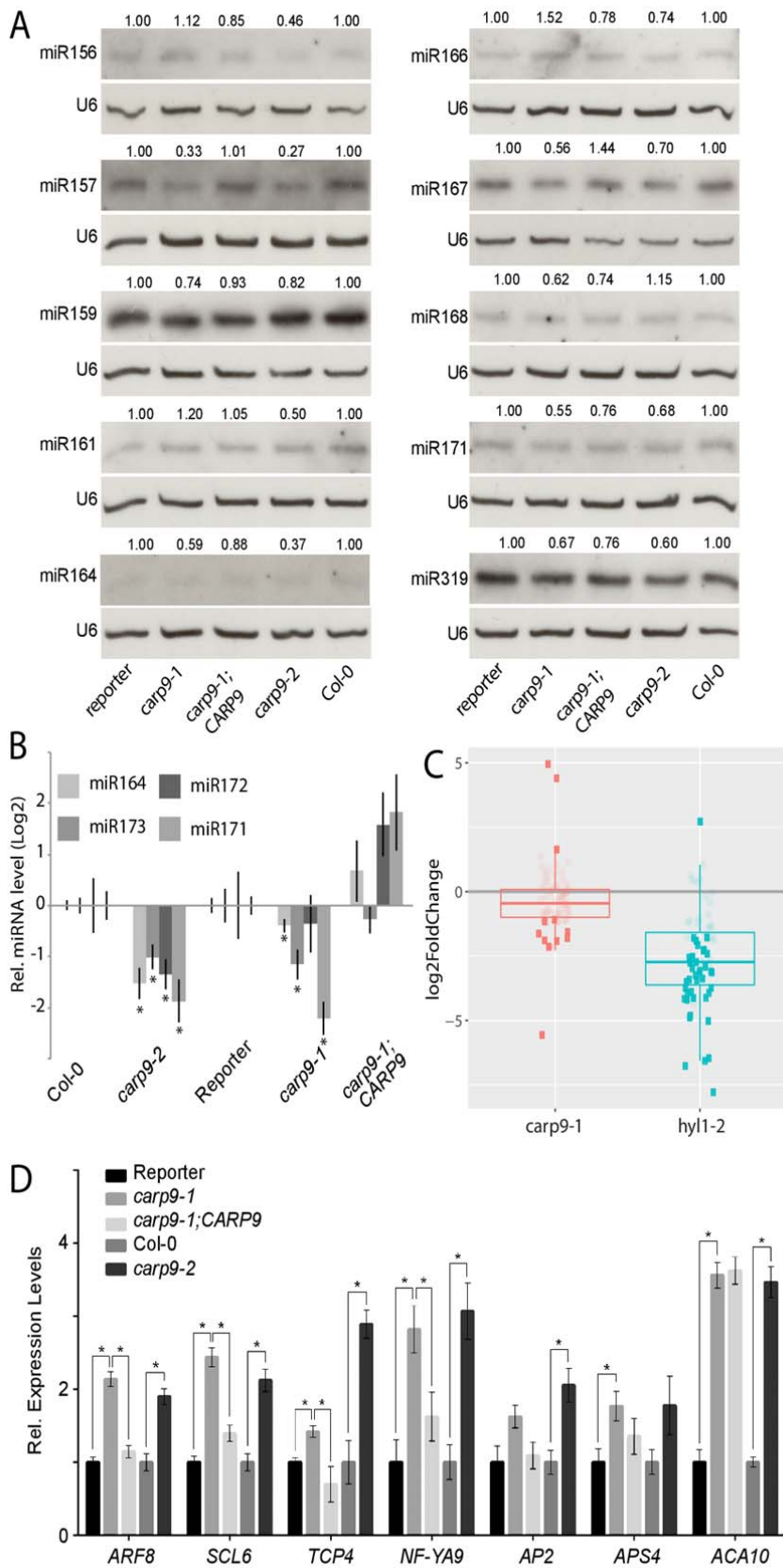
133 As *carp9-1* was isolated as a miRNA deficient mutant, we explored the endogenous levels of
134 several miRNAs by RNA blots and RT-qPCR. The quantification of miRNAs revealed a mild
135 reduction of several tested miRNAs in the single mutants, as well as in the *carp9-1/carp9-2*
136 compound heterozygous plants (Figure 2A, 2B, and Supplemental Figure S2A). As expected,
137 the overexpression of *CARP9* in *carp9-1* restored miRNA levels (Figure 2A and 2B). Aiming to
138 explore the genome-wide profile of miRNA accumulation in the *carp9* mutant, we performed
139 Illumina small RNA sequencing of *carp9-1* mutants. The results were consistent across
140 replicates (Supplemental Figure S2B) and supported our northern blot results. We observed an
141 overall reduction of miRNAs and miRNA*s accumulation, although to a lesser degree than
142 *hyl1-2* plants, used as controls of impaired miRNA production (Figure 2C, Supplemental Figure
143 S2C, Supplemental Table S1). Only the nuclear-acting miR845 (Borges et al., 2018), miR391,
144 and miR827 appeared over accumulated in *carp9-1* (Supplemental Table S1).

145 Coincidentally with impaired activity of the miRNA pathway in the mutants, we observed an
146 over-accumulation of several miRNA-targeted mRNAs in the single mutants and *carp9-1/carp9-2*
147 compound heterozygous plants (Figure 2D, Supplemental Figure S2D and S2E). As
148 expected, the *35S::CARP9* plants showed reduced miRNA-target transcripts to WT levels
149 (Figure 2D, and Supplemental Figure S2D).

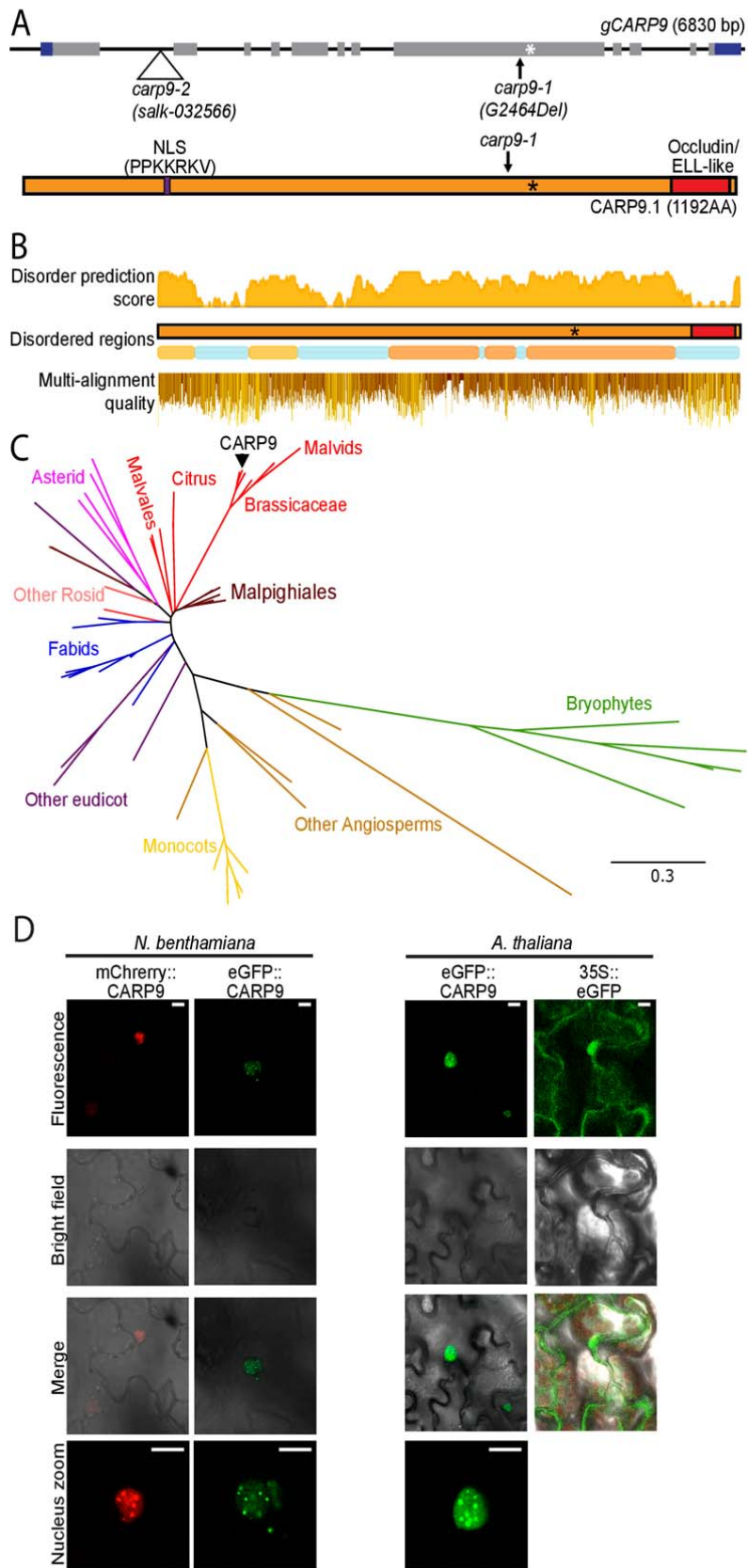
150

151 **CARP9 encodes an intrinsically disordered protein of unknown function conserved among** 152 **land plants**

153 *CARP9* encodes an 1192 amino acid long protein of unknown functions that includes a
154 predicted nuclear localization signal (NLS) at position 238-245 (Figure 3A). A single isoform is
155 reported in the TAIR10 genome version (Arabidopsis Genome, 2000), while a second splicing
156 variant is annotated in the Araport11 release (Cheng et al., 2017), but we were not able to detect
157 it by RT-PCR and represent less than the 2% of splicing junctions in RNA-seq experiments
158 (Supplemental Figure S3A). An analysis of the protein sequence searching for conserved
159 homology domains revealed only the presence of an Occludin/ELL-like domain (pfam E-value
160 score: 8.71e-27, (El-Gebali et al., 2019) in the C-terminal region, covering 8.4% of the total
161 protein length (amino acids 1088 to 1187, Figure 3A). Most of the eukaryotic RNA polymerase
162 II Elongation Factors (ELL) contain this kind of domains and are thought to mediate protein
163 interactions (Li et al., 2005; Van Itallie and Anderson, 2018), but they are mostly unstudied in
164 plants yet (Shilatifard et al., 1996). Besides this domain, a structure prediction indicated that
165 *CARP9* is an intrinsically disordered protein with 61.1% of disordered regions (Figure 3B)
166 (Potenza et al., 2015).



167 Interestingly, proteins with long disordered regions followed by an occluding domain appeared



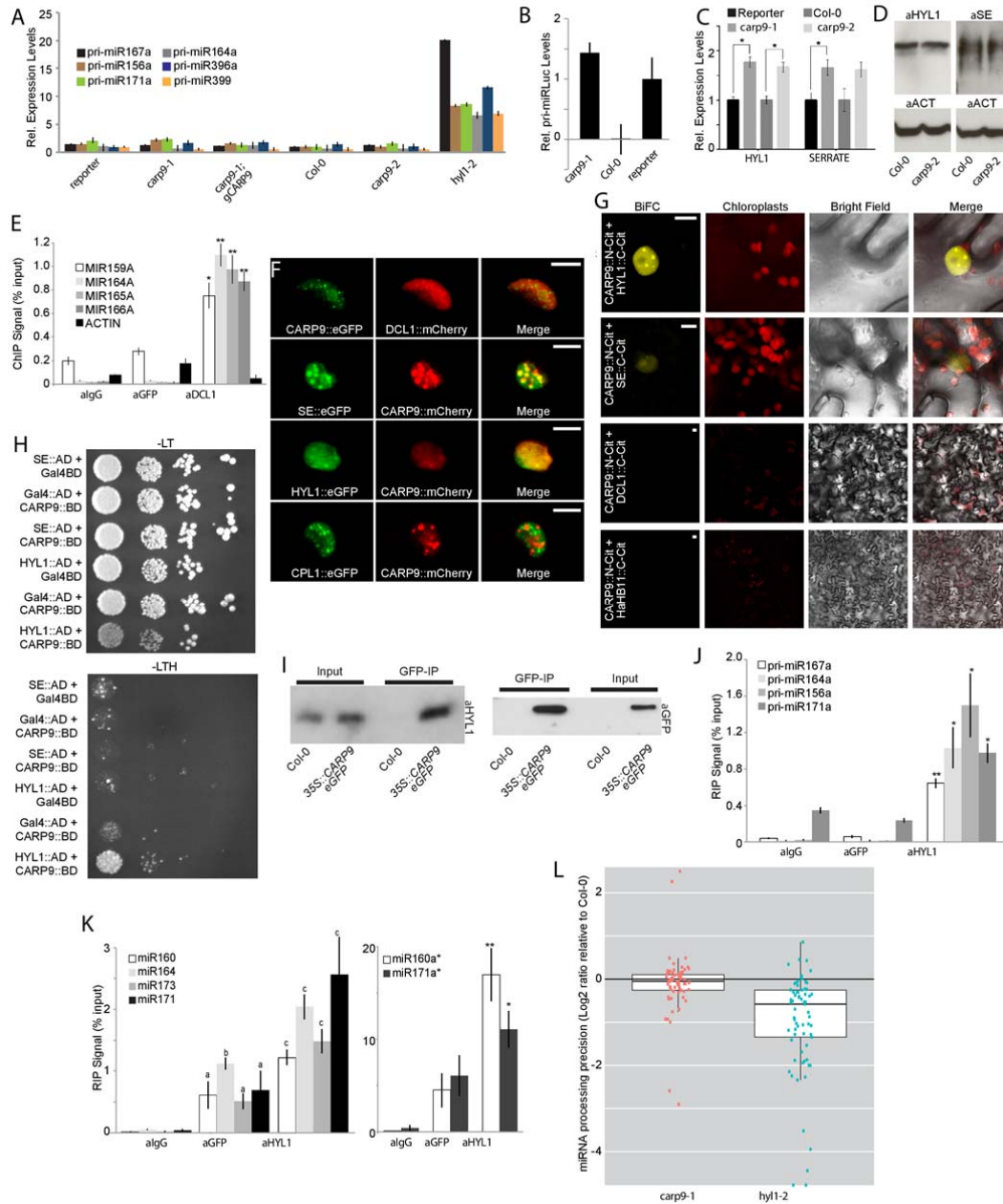
168 to be exclusive of plant species, according to the InterPro database (Mitchell et al., 2019). In this

169 sense, we performed a BLASTp search of CARP9 in plant genomes. This search yielded that
170 this gene is well conserved among embryophytes species (Figure 3C). We could also track
171 CARP9 orthologs in all embryophytes, including bryophytes, while they are absent in algae
172 species, suggesting that CARP9 has evolved within land plants. Using the Maximum Likelihood
173 method, we performed a phylogenetic analysis with these proteins (Figure 3C and Supplemental
174 Figure S3B). The obtained phylogenetic tree is entirely consistent with the evolution of plant
175 species and we did not identify conserved duplication events for this gene. In most of the
176 species, CARP9 orthologs correspond to a single-copy gene. Such a single copy of the gene
177 may explain why some of the studied alleles are not viable in homozygosis as redundancy may
178 be absent for this gene. However, we cannot exclude partial functional redundancy with other
179 IDPs. Proteins alignment showed that the conserved regions include both the Occludin/ELL
180 domain and the disordered region (Figure 3B). Moreover, CARP9 paralogs are also predicted as
181 disordered in all species. This suggests that both parts of the protein, the Occludin/ELL domain,
182 and the disordered region, might be necessary for their molecular function. IDPs are important
183 for molecular recognition (Tompa et al., 2015) and work as a scaffold for many molecular
184 interactions (Cortese et al., 2008). They are also particularly abundant in cellular membrane-less
185 organelles such as nuclear bodies (Uversky et al., 2015). Furthermore, intrinsically disordered
186 regions are essential in protein-RNA interactions, mediating both specific and non-specific
187 interactions (Varadi et al., 2015; Jarvelin et al., 2016). Recently, Arabidopsis FLL2, also a
188 disordered protein, was reported to be located in nuclear bodies promoting liquid-liquid phase
189 separation (Fang et al., 2019). The fusion of *CARP9* with the fluorescent proteins eGFP or
190 mCherry, followed by confocal microscopy, revealed that the protein localizes in the nucleus,
191 and particularly in nuclear bodies of unknown nature (Figure 3D and 3E). Such nuclear entities
192 could perfectly reflect specific liquid organelles or the well-known dicing-bodies, subnuclear
193 speckles of miRNA processing (Fang and Spector, 2007).

194

195 ***CARP9* interacts with HYL1 but does not affect miRNA processing**

196 The reduced miRNA levels in *carp9* mutants and the presence of an occludin/ELL domain in
197 CARP9 led us to propose a putative role as an elongation factor controlling the transcription of
198 genes encoding miRNA biogenesis factors or even of *MIRNA* genes. To test this hypothesis, we
199 first quantified by RT-qPCR transcript levels of pri-miRNAs and genes encoding core
200 components of the miRNA biogenesis machinery. In contrast to *hyl1-2* mutants, used as a
201 positive control for defective processing where pri-miRNAs over accumulate, *carp9-1* and
202 *carp9-2* presented normal levels of the miRNA precursors as well as pri-miRLUC (Figure 4A
203 and 4B). Among all tested genes encoding miRNA related proteins, we observed a subtle but
204 significant increase in HYL1 and SE transcript levels (Figure 4C). This result is opposed to our
205 hypothesis of CARP9 acting as an elongator factor but compatible with a feedback response to



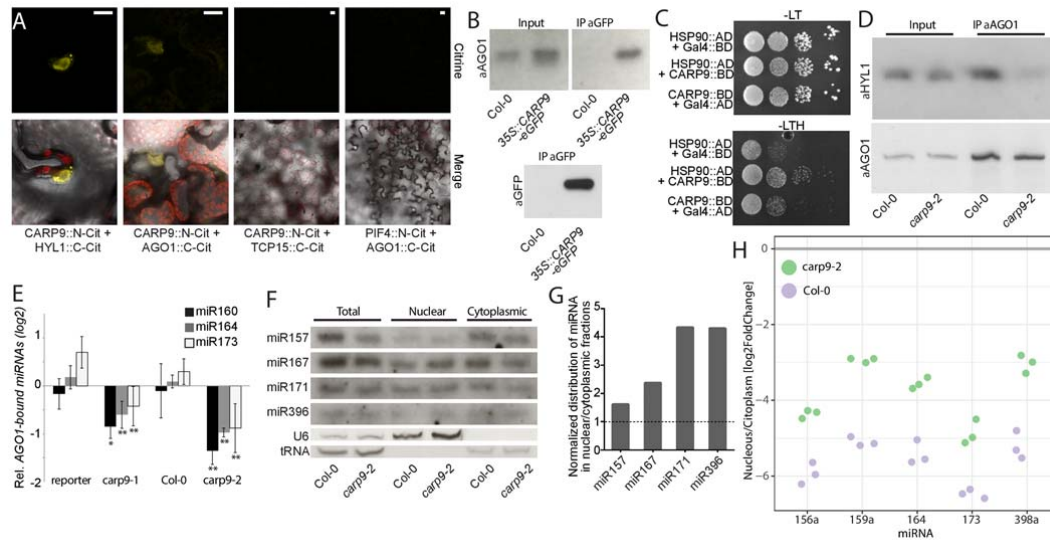
206 the impaired miRNA activity in the mutants. However, immunoblot analysis of HYL1 and SE
 207 showed that these protein levels remained stable in the mutants (Figure 4D). It has also been
 208 shown that DCL1 is recruited to *MIRNA* genes by the action of elongation factors (Fang et al.,
 209 2015). Thus, it is possible that CARP9 does not affect *MIRNA* genes transcription itself but
 210 allows the recruitment of the processing machinery to the *loci*. We tested the capacity of
 211 CARP9 to interact with *MIRNA loci* by ChIP-qPCR using an eGFP-tagged version of the
 212 protein. Unlike DCL1, used as a positive control, CARP9 did not appear associated with the
 213 tested *MIRNA loci* (Figure 4E). Altogether, these results suggested that CARP9 is not acting as
 214 an elongator factor to control miRNA activity. Alternatively, it is also possible that CARP9 is

215 directly implicated in the processing of pri-miRNA, based on its particular sub-nuclear
216 localization in speckles similar to dicing bodies (Figure 3D and 3E). Interestingly, transient
217 expression of fluorescent-tagged CARP9 followed by confocal microscopy showed
218 colocalization with SE and HYL1 in the same nuclear speckles (Figure 4F). However, it did not,
219 or only partially, colocalized with DCL1 and CTD-PHOSPHATASE-LIKE 1 (CPL1), which
220 de-phosphorylate HYL1 to enhance pri-miRNA processing (Figure 4F). Coincidentally,
221 bimolecular fluorescence complementation (BiFC) assays showed fluorescent reconstitution
222 when *CARP9::N-CITRINE* was confronted with HYL1 and SE fused to the *C-CITRINE*, but not
223 with DCL1 (Figure 4G and Supplemental Figure S4). We used the nuclear transcription factor
224 HaHB11 (Cabello et al., 2016) as a negative control for the assay. Since colocalization and
225 BiFC assays indicate protein proximity but not necessarily interactions, we performed a yeast
226 two-hybrid assay (Y2H) to evaluate direct protein-protein interaction between CARP9, HYL1,
227 and SE. Only HYL1 among the tested proteins was able to interact with *CARP9* (Figure 4H).
228 This interaction was further confirmed by a Co-IP experiment using eGFP tagged CARP9 and
229 an antibody against the endogenous HYL1 (Figure 4I). The fact that HYL1 is known to interact
230 with SE (Lobbes et al., 2006), may explain the positive signal detected between SE and CARP9
231 in BiFC assays. RIP-qPCR assays using a GFP-tagged CARP9 showed no association of this
232 protein with pri-miRNAs, which appeared associated to HYL1 (Figure 4J). Conversely, we
233 detected abundant mature miRNAs associated with CARP9 in the IP samples (Figure 4K). This
234 association of CARP9 with mature miRNAs is probably through its interaction with HYL1,
235 which is known to interact with miRNAs (Yang et al., 2010). The fact that HYL1 binds both
236 pri-miRNA and mature miRNAs (Figure 4J and 4K, and Yang et al., 2010) but CARP9 only
237 appeared to interact with mature miRNA suggests that CARP9-HYL1 interaction occurs after
238 pri-miRNA processing. Supporting this scenario, miRNA-processing precision, a feature
239 impaired in *hyll-2* mutants and associated to its function as DCL1 accessory protein, was not
240 affected in *carp9-1* plants (Figure 4L). MiRNA processing precision was calculated by scoring
241 the ratio of total miRNA-matched small RNA to the pool of imprecisely processed small RNAs,
242 defined as those only partially matching the mature miRNA sequence. A late action of CARP9
243 in the pathway is also in line with the lack of interaction of CARP9 with DCL1 and CPL1,
244 which are expected to act on early stages of the miRNA processing. This is also in agreement
245 with the unchanged levels of pri-miRNAs in the mutant compared to WT (Figure 4A), which
246 tend to accumulate in mutants impair in pri-miRNA processing (Ben Chaabane et al., 2013),
247 suggesting that CARP9 is not active during miRNA biogenesis.

248

249 ***CARP9* interacts with AGO1, affects its stability and miRNA loading**

250 The potential post-miRNA-processing interaction of CARP9 with HYL1, and its nuclear
251 localization, suggested that this protein might affect one of the nuclear steps of the miRNA



252 pathway downstream of biogenesis. This could be the case of the recently reported nuclear
 253 loading of some miRNAs into AGO1 (Bologna et al., 2018). To explore this possibility, we first
 254 tested the capacity of CARP9 to interact with AGO1 by BiFC and Co-IP assays. Both
 255 experiments showed that CARP9 can interact with AGO1, and this interaction occurs in the
 256 nucleus, as observed in the microscopy assays (Figure 5A, 5B, Supplemental Figure S5A, and
 257 S5B). The nuclear transcription factors TCP15 and PIF4 (Ferrero et al., 2019) were used as
 258 negative controls for the assay. Interestingly, Y2H assays showed that CARP9 also interacts
 259 with the known AGO1-partner HSP90, which can locate in the nucleus (Bologna et al., 2018)
 260 (Figure 5C). Contrary, BiFC assays revealed that CARP9 do not interact with SQUINT, which
 261 according to our data, interacts with AGO1 exclusively in the cytoplasm (Supplemental Figure
 262 S5C). As CARP9 interacts with HYL1, and this protein was shown to interact with AGO1 in the
 263 nucleus (Fang and Spector, 2007), it is possible that CARP9, as many intrinsically disordered
 264 proteins, acts as a scaffold for AGO1-HYL1 interaction. To test this hypothesis, we performed
 265 AGO1-HYL1 co-IP experiments in WT and *carp9-2* mutants treated with the proteasome
 266 inhibitor MG132. MG132 treatments equalize AGO1 levels, which are altered in *carp9* mutants
 267 (see below), allowing us a correct interpretation of the results. The experiment showed that
 268 AGO1-HYL1 interaction is partially impaired in the mutant background suggesting that CARP9
 269 facilitates the formation of a post-processing miRNA complex containing AGO1, HYL1, and
 270 likely HSP90 (Figure 5D and Supplemental Figure S5D).

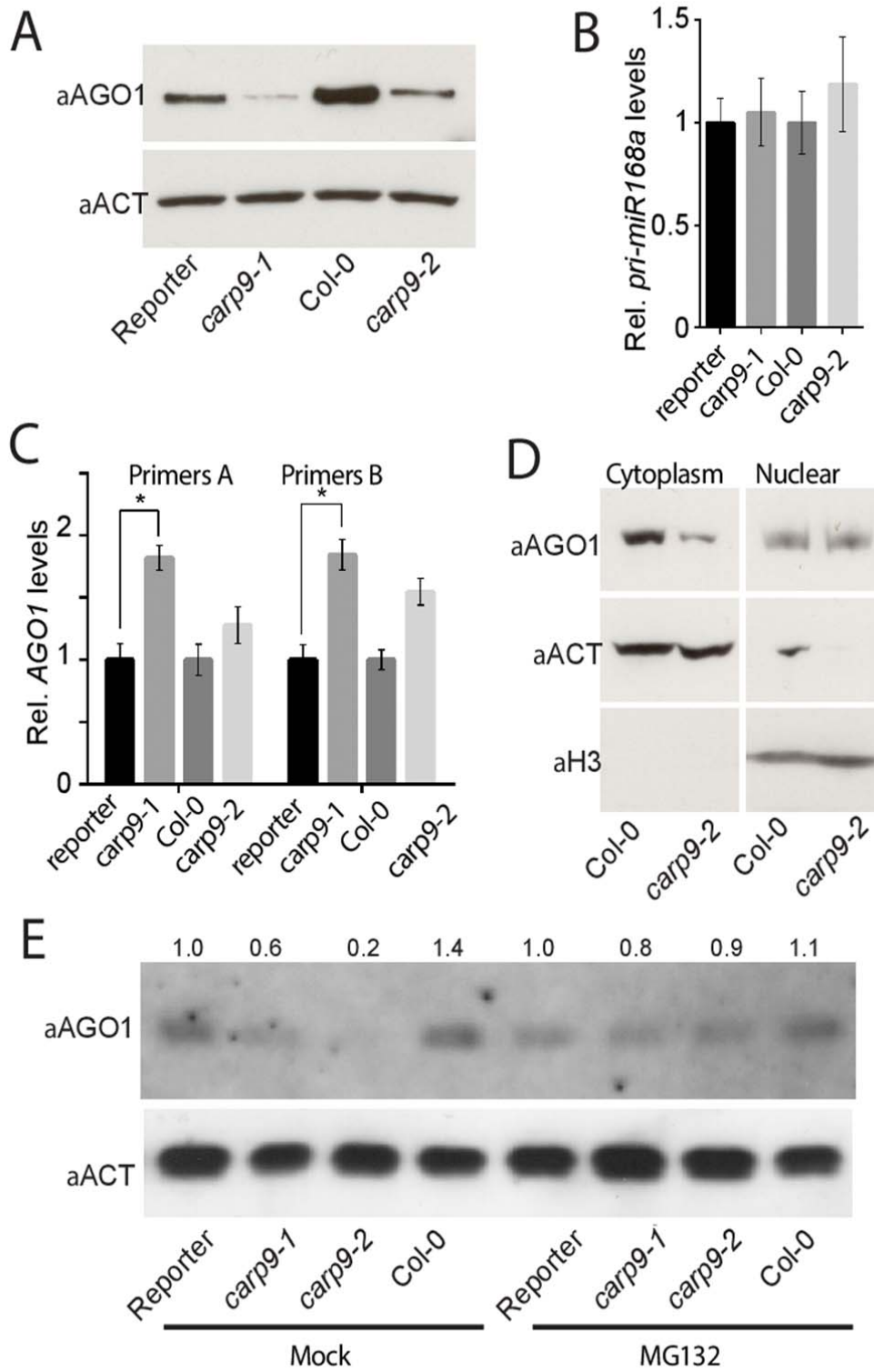
271 Altogether this data suggests that CARP9 may act stabilizing HYL1-AGO1 interaction and
 272 perhaps facilitating the loading of miRNAs into AGO1. To test whether AGO1 loading is
 273 affected in *carp9* mutants, we immunoprecipitated AGO1 in WT and mutant plants treated with
 274 MG132 and scored the levels of associated miRNAs by RT-qPCR (RIP-qPCR). We observed a
 275 significant depletion of AGO1-associated miRNAs in the mutants when compared to WT

276 plants, except for miR822 that is canonically loaded in the cytoplasm ((Rajagopalan et al.,
277 2006), Figure 5E, Supplemental Figure S5E and S5F), suggesting that CARP9 is participating in
278 the nuclear loading of miRNAs into AGO1 or at least stabilizing AGO1-miRNA association.
279 This observation may explain the mild reduction in miRNA accumulation as most likely *carp9*
280 mutation only affect the portion of miRNAs loaded in the nucleus but not the cytoplasmic
281 loading. The impaired loading of miRNAs into AGO1 in *carp9* mutants was also evident when
282 we measured mature miRNAs accumulation in nuclear and cytoplasmic fractions. RNA blot and
283 RT-qPCR assays revealed that the nuclear portion of mature miRNAs is enriched in *carp9-2*,
284 compatible with deficient AGO1 nuclear loading, and subsequent cytoplasm exportation of this
285 miRNA fraction (Figure 5F, 5G, 5H, and Supplemental Figure S5G).

286 Intriguingly, we detected increased levels of AGO1 in the plants overexpressing eGFP:CARP9
287 construct (Figure 5B and Supplemental Figure S5B) and a reduction in *carp9-1* and *carp9-2*
288 mutants when compared to their respective controls (Figure 6A). Such changes in AGO1 levels
289 cannot be attributed to the known regulation of *AGO1* by miR168 (Vaucheret et al., 2004), as
290 we did not observe an increment of miR168 or *MIR168* transcript levels (Figure 1E, 6B, and
291 Supplemental Table S1). In contrast to AGO1 protein, *AGO1* transcripts levels, measured by
292 RT-qPCR with primers designed toward the 3' end of the mRNA (primers set A) or flanking the
293 miR168 target site (primers set B), were higher in the mutants than in control plants probably as
294 a feedback response to the protein reduction or as a consequence of the lower miR168 activity
295 (Figure 6C, Supplemental Table S1). Nuclear/cytoplasm protein fractionation of WT and *carp9-2*
296 plants showed that the nuclear fraction of AGO1 is not reduced in the mutant, which is
297 consistent with a possible cytoplasmic proteolytic degradation of AGO1 (Figure 6D). Treatment
298 of the mutant plants with the proteasome inhibitor MG132 partially reverted AGO1 reduction
299 confirming that this protein is being degraded in the mutants (Figure 6E and Supplemental
300 Figure S6). Such reduced levels of AGO1 can be the cause, but also the consequence of the
301 deficient miRNA loading observed in the mutants as unloaded AGO1 could become unstable
302 and get degraded. Nevertheless, the most parsimonious explanation to our observations is that
303 CARP9 is acting as a scaffold protein promoting the formation of a nuclear post-processing
304 miRNA complex containing at least AGO1, HYL1 and HSP90. In the absence of CARP9 this
305 hypothetical complex would be disrupted thus altering AGO1 stability, the proper miRNA
306 loading and therefore the stability of miRNA duplex itself.

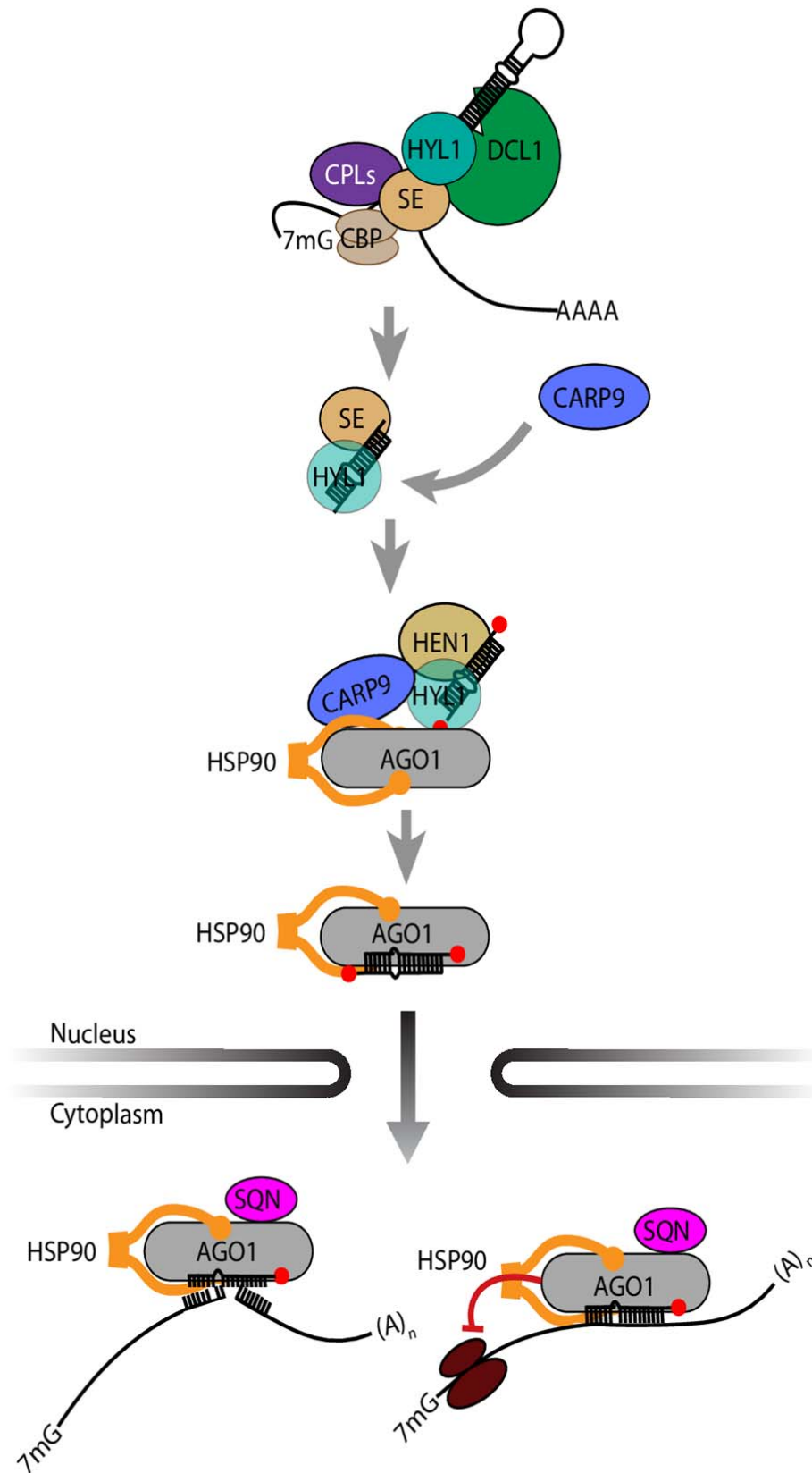
307

308



310 During the last years, our knowledge of the miRNA pathway in plants has grown exponentially.
311 New functions were assigned to well-known proteins of the pathway, such as the chromatin
312 association of AGO1 and DCL1 (Fang et al., 2015; Dolata et al., 2016; Liu et al., 2018), the role
313 of these same proteins in DNA damage repair (Wei et al., 2012; Schalk et al., 2017), the
314 transcriptional and epigenetic regulation of genes by SE (Ma et al., 2018; Speth et al., 2018),
315 and the independence of some pri-miRNA of HYL1 at low temperatures (Re et al., 2019),
316 among other examples. A recent report demonstrated that a portion of miRNAs can be directly
317 loaded into AGO1 inside the nucleus and exported as a complex (Bologna et al., 2018). This
318 evidence contrasts the previous conception that miRNAs were exported to the cytoplasm by
319 HASTY in order to be loaded into AGO1. The functional relevance of AGO1 nuclear loading is
320 becoming important since AGO1 involvement in several nuclear processes were recently
321 described (Dolata et al., 2016; Schalk et al., 2017; Liu et al., 2018). However, it remains
322 unknown whether this nuclear loading of AGO1 is a passive process or if components of the
323 processing machinery assist it. It has been previously shown that proper loading of AGO1,
324 particularly the miRNA strand selection, is impaired in *HYL1* mutants, suggesting that this
325 processing factor might participate actively during AGO1 loading (Eamens et al., 2009;
326 Manavella et al., 2012). Interestingly HEN1, which 2' -O-methylates mature miRNA, interacts
327 with HYL1, but not with the processing factor SE (Baranauske et al., 2015). This potentially
328 also place HEN1 in an hypothetical post-processing complex together with AGO1 and HYL1.
329 The capacity of HYL1 to efficiently bind mature miRNAs *in vitro* (Yang et al., 2010), suggests
330 that, after processing, mature miRNA might remain bound to HYL1 until loaded into AGO1. In
331 this context CARP9 appeared to act as a nexus among these proteins facilitating the proper
332 function of such post-processing complex (Figure 7).

333 In this study, we describe CARP9, an intrinsically disordered protein conserved among land
334 plants, as a nuclear protein participating in miRNA activity. Interestingly, we found that CARP9
335 interacts with HYL1 and mature miRNAs but not with the miRNA processing machinery or
336 miRNA precursors, suggesting that this protein functions after the pri-miRNA processing steps.
337 This idea is strongly supported by a miRNA-processing precision analysis that showed that
338 *carp9-1* mutants, opposite to *hyl1-2*, displayed a normal processing activity (Figure 4L). This
339 discovery also supports previous reports proposing that HYL1 remains bound to the mature
340 miRNA duplexes once they are produced (Figure 5, (Baranauske et al., 2015). In this context, it
341 is possible that after pri-miRNA processing, HYL1 transfers the mature miRNA duplexes to
342 AGO1 in the nuclear speckles where they colocalize, a scenario compatible with the AGO1
343 loading defects in *hyl1* mutants (Fang and Spector, 2007; Eamens et al., 2009; Manavella et al.,
344 2012). Furthermore, HYL1 may facilitate AGO1 loading in the cytoplasm, where it is also
345 located without reported functions (Cho et al., 2014; Achkar et al., 2018). However, and to the
346 best of our knowledge, there is no evidence of direct interaction between HYL1 and AGO1 in



347 the cytoplasm. Besides its interaction with HYL1, we found that CARP9 also interacts with

348 AGO1 contributing to the miRNA loading process (Figure 5). It is common that IDPs, as
349 CARP9, act as chaperones assisting the folding of other proteins, allowing interactions and even
350 preventing their aggregation (Tompa and Kovacs, 2010). In such a scenario, CARP9 could act
351 as a scaffold promoting AGO1-HYL1 interaction, providing stability to AGO1 and to the
352 mature miRNA duplexes and consequently promoting loading of miRNA into AGO1. As HYL1
353 is also found in the cell cytoplasm, where it undergoes protein degradation during the night
354 (Cho et al., 2014; Achkar et al., 2018), it is possible that this RNA binding protein escort AGO1
355 during miRNA nuclear export, a process that would exclude CARP9 as we found it to be
356 exclusively nuclear.

357 It was interesting to notice that *carp9* mutant alleles displayed reduced AGO1-bound miRNAs,
358 miRNA levels, and morphological defects compatible with miRNA deficient mutants. However,
359 these defects are milder than the observed in mutants of core proteins of the pathway, such as
360 HYL1 and AGO1. Redundancy with proteins with high sequence similarity is unlikely to
361 explain this observation as CARP9 appeared as a single gene in most of the genomes of plants
362 considered here, including Arabidopsis and by the fact that plants homozygous for *carp9* null
363 alleles appeared not to be viable. It is more likely that a reduced activity of CARP9 in the
364 mutant alleles explains the observations, as the premature stop codon in *capr9-1* would allow a
365 large portion of the protein to be translated and the intronic T-DNA insertion of *carp9-2*
366 possibly represents a knock-down allele as indicated by the reduced *CARP9* transcripts in this
367 mutant (Supplemental Figure S3). Besides, as CARP9 is likely to only affect the nuclear loading
368 of miRNAs, the large pool of cytoplasmic loaded miRNAs are not expected to be affected, thus
369 restricting the effect of the protein to only a subpopulation of miRNAs.

370 It is notable the high degree of conservation of CARP9 among land plants suggesting a crucial
371 role of this protein for plant homeostasis. The extraordinary level of amino acid conservation in
372 the intrinsically disordered regions, which commonly tend to diverge rapidly during evolution
373 rapidly, reinforce the idea of an evolutionary pressure to conserve this protein. Such inference
374 might explain why we failed to identify homozygous T-DNA mutants in the coding sequence of
375 this gene. The identification of strong but viable loss-of-function alleles of *CARP9* could help to
376 dimension the importance of this protein in plant development and miRNA processing in the
377 future.

378 CARP9 represents a new component of the miRNA pathway that links the post-processing
379 machinery with the miRNA effector complex. Several questions remain open; for example,
380 HEN1 was shown to interact with HYL1 post-processing (Baranauske et al., 2015), opening the
381 question of whether AGO1 is loaded with already methylated miRNA or if such process occurs
382 after loading for the fraction of nuclear-loaded miRNAs. EMA1 and TRN1 were also shown to
383 interact with AGO1 modulating miRNAs loading (Wang et al., 2011; Cui et al., 2016).
384 However, it remains to be addressed whether these proteins also participate in the nuclear

385 AGO1-loading process interacting with HYL1 and CARP9 or have a different role. Similarly,
386 we showed that CARP9 interacts with AGO1 and HYL1 to facilitate loading, but the
387 biochemical activity of CARP9 during this process is unclear. Perhaps the most intriguing
388 question lays in the observed destabilization of AGO1 in *carp9* mutants. How this process is
389 triggered and accomplished are questions we still need to answer. In particular, it will be
390 essential to understand how AGO1 degradation, CARP9-HYL1 interaction, and miRNA loading
391 are interconnected.

392 We found three significant effects of *carp9* mutations; a mild reduction in miRNAs levels, a
393 reduction in AGO1 loading, and a reduction in AGO1 protein levels. Interestingly, each of these
394 observations can be explained in light of the other ones. In this sense, miRNA reduction and
395 impaired AGO1 loading can be the consequence of AGO1 destabilization. It is also possible that
396 impaired AGO1 loading destabilizes AGO1 and miRNAs. Finally, if CARP9 is directly
397 involved in stabilizing the miRNA duplex after processing, we could also expect to see impaired
398 AGO1 loading and stability. Perhaps the first scenario is the less likely as AGO1 loading is
399 impaired in *carp9* even when MG132 treatments block protein degradation. Nevertheless, we
400 cannot exclude any of these possibilities, and further studies will be necessary to discriminate
401 these alternatives and to understand the role of CARP9 in HYL1-AGO1 crosstalk precisely.

402

403 **MATERIALS AND METHODS**

404 **Plant Material and Growth Conditions**

405 *Arabidopsis* (*Arabidopsis thaliana*) ecotype Columbia (Col-0), reporter and mutant plants were
406 grown at 23°C on soil in long-day photoperiod (LD, 16 hours of light/8 hours of dark).
407 Alternatively, plants were grown on plates containing 2.2 g/L of Murashige and Skoog (MS)
408 medium (pH 5.7) and 0.6% (w/v) agar in LD conditions. Seeds were disinfected with 10% (v/v)
409 bleach and 0.1% (w/v) SDS and stratified in 0.1% (w/v) agar for 3 days at 4° C before sowing.
410 Mutant lines *carp9-2* (SALK_032566); *capr9-3* (SALK_060892), *carp9-4* (SALK_044585),
411 *carp9-5* (WiscDsLox358B04) and *hyl1-2* (SALK_064863) were obtained from ABRC stock
412 center. Col-0 miRNA activity reporter lines (reporter) used for EMS mutagenesis, and thus as
413 *capr9-1* control, were previously described (Manavella et al., 2012). Transgenic lines were
414 grown on MS plates with 50 mg/mL kanamycin.

415

416 **DNA Constructs and Plant Transformation**

417 The *CARP9*, *HSP90*, *SQN* coding region sequences (CDS), with or without stop codon, were
418 amplified and cloned into pEntr/D-TOPO or pCR8GW-TOPO entry vector (Thermo Fisher
419 Scientific). The *CARP9* promoter region (2558 bp upstream the transcription start site) was

420 amplified by PCR, fused to *CARP9* cDNA fragment by PCR, and cloned into pEntr/D-TOPO
421 entry vector. EGFP and mCherry fusion constructs were obtained by recombination of the entry
422 clones into modified pGREEN vectors under the control of the CaMV 35S promoter. An
423 untagged cDNA copy of *CARP9* under a 35S promoter was used to rescue *carp9-1* mutants.
424 Yeast two-hybrid constructs were obtained by cloning the specific cDNAs into pEntr/D-TOPO,
425 followed by recombination into the pDEST32 or pDEST22 vectors (Life Technologies). Refer
426 to Supplemental Table S2 for a detailed list of constructs used in this work. Arabidopsis
427 transgenic seedlings were selected using 50 mg/ml kanamycin on plates. At least 15
428 independent pooled T1 seedlings were used for quantitative measurement of transgenic lines.
429 Transient infiltration of *Nicotiana benthamiana* leaves was performed as described previously
430 (de Felippes and Weigel, 2010). We were unable to directly transform *carp9* mutants by floral
431 dip. Thus all *carp9* transgenic plants were obtained by crossing the mutants with transgenic Col-
432 0 plants and then recover the homozygosis on the mutant alleles. In the case of the experiments
433 performed with overexpression lines we only used plants with low expression levels of *CARP9*
434 and pooled lines to minimize variability.

435

436 **RNA Analysis**

437 Total RNA was extracted from 15-days-old plants using TRIzol reagent (Life Technologies).
438 For RNA blots, 1-5 µg of total RNA were resolved in 17 % (v/v) polyacrylamide gels under
439 denaturing conditions (7 M urea) and then transferred to HyBond-N+ charged nylon membranes
440 (Amersham) by semidry electroblotting (Tomassi et al., 2017). RNA was covalently fixed to
441 membranes in a UV Crosslinker. Membranes were hybridized overnight with DNA
442 oligonucleotide probes labeled with second-generation DIG Oligonucleotide 3'-End Labeling
443 Kit (Roche); the signal was detected using CSPD ready-to-use solution, by exposure to
444 Amersham hyperfilm ECL (GE Healthcare Life Sciences). ImageJ was used to analyze the band
445 intensity of small RNA blots as integrated pixel density, using the intensity of U6 bands to
446 normalize sample loading. Reverse transcriptase reactions were performed using 1 µg of
447 DNaseI-treated total RNA (Thermo Fisher Scientific) using the RevertAid RT Reverse
448 Transcription Kit (Thermo Fisher Scientific). Quantitative RT-qPCRs, were performed using
449 three independent biological replicates of pooled seedlings, and ACTIN2/8
450 (At3g18780/At1g49240) were used as a housekeeping loading control. Stem-Loop RT-qPCRs
451 for miRNAs quantification were performed as previously described (Kramer, 2011). Averages
452 from biological triplicates and SE were calculated from $2^{-\Delta\Delta Ct}$ values, and the error displayed as
453 two times SM. Each replicate was treated as independent samples for statistical analysis.
454 Statistical differences between samples were determined by an unpaired, two-tailed, *t*-test
455 analysis and corrected with Holm-Sidak method for multiple pair comparisons. All

456 quantifications were repeated twice in independent experiments. See Supplemental Table S3 for
457 oligonucleotide primer and probe details.

458

459 **Small RNA sequencing**

460 Small RNA libraries were prepared as indicated by the TruSeq small RNA library prep kit
461 (Illumina) using biological triplicates of the reporter lines and *hyl1-2* mutants and duplicates of
462 *carp9-1* mutants. 50 ng of small RNAs purified with the ZR small-RNA PAGE Recovery Kit
463 (Zymo Research) were used as input for the library preparation. Small RNA libraries size
464 selections were performed using the BluePippin System (SAGE Science). Single-end Illumina
465 sequencing was performed with a HiSeq3000 apparatus. Small RNA reads were first processed
466 to remove 3' adapters using cutadapt (version 1.9.1) and then mapped using bowtie (version
467 1.1.2). Reproducibility was tested by computing the Spearman correlation of the miRNA counts
468 per million between all samples, converting this correlation to a distance (1-Spearman Rho) and
469 performing a hierarchical clustering of the samples, with the "complete" agglomeration method,
470 to show the degree of similarity between them. The references used were the databases for
471 hairpin and mature miRNAs for *A. thaliana* from miRBase (release 21), in the latter mature
472 miRNAs with identical sequences were collapsed into single miRNAs. Additionally, reads were
473 mapped to the *A. thaliana* genome using the same software. For the differential expression
474 analysis of the miRNAs, only reads mapping to the full-length mature miRNAs were
475 considered, and primary alignments of reads mapping to the sense strand were counted (filtering
476 with "samtools view-F 272"). Counts per miRNA were used as input for baySeq (version 2.8.0)
477 to perform the differential expression analysis. For this, miRNAs with low expression levels
478 (less than 10 counts in all samples) were discarded, and size factors were set according to the
479 total number of reads mapping to the genome for each sample. Graphics and statistical analyses
480 were performed in the R statistical programming environment (R Core Team, 2018) with the
481 ggplot package. MiRNA processing precision was calculated by scoring the ratio of total
482 miRNA-matched small RNA to the pool of imprecisely processed small RNAs, defined as those
483 only partially matching the mature miRNA sequence. All data reported in this paper is available
484 at the European Nucleotide Archive (ENA), PRJEB37499.

485

486 **Protein Analysis**

487 For immunoblot analysis, proteins were extracted from 15-days-old pooled plants (n=5) with
488 100 µl extraction buffer (50 mM Tris pH 7.5, 150 mM NaCl, 1 mM EDTA, 10% (v/v) Glycerol,
489 1 mM DTT, and one tablet Complete Protease Inhibitor Cocktail [Roche]) per 100 mg of grind
490 tissue. Proteins were resolved in 8% (w/v) SDS-PAGE gels (running buffer: 25 mM Tris-Base;

491 192 mM Glycin; 0.1% (w/v) SDS) and transferred using a standard wet tank blotting (blotting
492 buffer: 2.5 mM Tris-Base; 19.2 mM Glycine; 10% (v/v) methanol) to PVDF membrane
493 (Amersham). Thermo Scientific PageRuler Prestained Protein Ladder was used to determine the
494 molecular weight of the bands and to confirm transfer efficiency. AGO1, HYL1, and SE were
495 detected using a polyclonal antibody targeting the endogenous Arabidopsis protein (Agrisera
496 AS09527, AS06136, and AS09532; dilution 1:10,000 each). ACTIN 8 (Agrisera AS132640;
497 dilution 1:10,000), HISTONE3 (Agrisera AS10710; dilution 1:10,000), or coomassie blue
498 staining, were used as loading controls in different experiments. HBR-conjugated polyclonal
499 anti-rabbit IgG, (Agrisera AS09602; dilution 1:20,000), was used to detect primary antibodies.
500 Signal was detected using ECL Plus Western Blotting Substrate (Thermo Fisher Scientific).
501 Experiments were repeated at least twice. For Co-IP assays, eGFP-CARP9 was
502 immunoprecipitated with an anti-GFP antibody (ABCAM ab290, dilution 1:1000) from samples
503 extracted from transgenic *A. thaliana* flowers transformed with 35S::eGFP:CARP9 including
504 WT Col-0 flowers as a negative control, and AGO1 was immunoprecipitated with an anti-
505 AGO1 antibody (Agrisera, dilution 1:1000) from samples extracted from pooled (n=5) 15-days-
506 old *carp9-1*, *carp9-2*, reporter and WT Col-0 plants, using Sure Beads™ Protein-A magnetic
507 beads (BioRad) following the manufacturer's instruction. eGFP:CARP was then detected in the
508 input and IP fraction by immunoblot using an anti-GFP antibody (ABCAM ab290, dilution
509 1:10000). HYL1 and AGO1 were detected in the input and IP fraction using the antibodies
510 previously described. Yeast two-hybrid assays were performed with the ProQuest Two-Hybrid
511 System (Thermo Fisher Scientific). Selection medium containing 2.5 mM of 3-AT (3-amino-
512 1,2,4-triazole) was used to detect interactions reducing autoactivation. CARP9 fusions to the N-
513 terminal and C-terminal fragments of Citrine, eGFP or mCherry were used for BiFC assays, and
514 protein localization in transiently transformed *N. benthamiana* leaves. Fluorescent protein
515 visualization and imaging were performed using a Leica TCS SP8 confocal microscope. The
516 excitation wavelengths were 488 nm, 514 nm, and 552 nm, and emission was collected at 500-
517 530 nm, 525-560 nm, and 600-630 nm for eGFP, mCitrine, and mCherry, respectively. For
518 Luciferase activity assays, twelve 5mm discs cut from mature leaves were individually
519 embedded in 100 mM D-Luciferin potassium salt solution and bioluminescence quantified using
520 a Fluoroskan Ascent™ FL plate Luminometer (Thermo Scientific). Means and SE was
521 calculated (n=12) and p-values of less than 0.05 in a two-tailed, unpaired t-test Holm-Sidak-
522 corrected, were considered significant. Alternatively, Luciferase activity was detected in plants
523 sprayed with 100 mM D-Luciferin potassium salt solution using an Orca 2-BT cooled CCD
524 camera with 5 minutes integration time (Hamamatsu Photonics).

525

526 Nuclear-Cytoplasmic Fractionation

527 Nuclear/cytoplasmic fractionation was performed following a protocol previously described
528 (Wang et al., 2011). Briefly, samples of pooled 15-days-old plants (2.5 g) were ground on ice
529 with 2 ml/g of lysis buffer (20 mM Tris-HCl pH 7.5, 20 mM KCl, 2 mM EDTA, 2.5 mM
530 MgCl₂, 25% (v/v) glycerol, 250 mM Sucrose, and 5 mM DTT) supplemented with 200 μM
531 PMSF (only for proteins fractionations). The homogenate was filtered through a layer of
532 Miracloth, and the flow-through was centrifuged at 1,500 g for 10 minutes. The supernatant
533 (cytoplasmic fraction) was centrifuged at 10,000 g and 4° C for 10 minutes, and collected. The
534 pellet was washed 3-5 times with 5 mL of NRBT buffer (20 mM Tris-HCl pH 7.5, 25% (v/v)
535 glycerol, 2.5 mM MgCl₂, and 0.2% (v/v) Triton X-100) and then resuspended with 500 μL of
536 NRB2 (20 mM Tris-HCl pH 7.5, 0.25 M Sucrose, 10 mM MgCl₂, 0.5% (v/v) Triton X-100, and
537 5 mM β-mercaptoethanol) supplemented with Complete Protease Inhibitor Cocktail (Roche,
538 only for protein fractionations). The resuspension was carefully pipetted on top of 700 μL of
539 NRB3 buffer (20 mM Tris-HCl pH 7.5, 1.7 M Sucrose, 10 mM MgCl₂, 0.5% (v/v) Triton X-
540 100, and 5 mM β-mercaptoethanol, supplemented with Complete Protease Inhibitor Cocktail).
541 The obtained sucrose gradient was centrifuged at 16,000 g and 4° C for 1-3 minutes. For protein
542 extraction, the pellet was resuspended in 100 μL lysis buffer and sonicated in a Bioruptor Pico
543 water bath (10 cycles of 30 seconds on/30 seconds off pulses at high intensity) (Diagenode).
544 After centrifugation at 16,000 g for 10 min at 4° C, the supernatant was collected as the nuclear
545 fraction. For RNA extraction, the pellet was resuspended in 200 μL lysis buffer, and then 1 mL
546 of TRIzol reagent (Life Technologies) was added, as to the cytoplasmic fraction, following then
547 by a standard protocol for RNA extraction. As a quality and loading controls for the
548 fractionation, ACTIN 8 and a tRNA probe (for RNA quantifications) were used as cytoplasmic
549 markers, while Histone H3 and U6 RNA (for RNA quantifications) were used as nuclear
550 markers.

551

552 **RNA and Chromatin Immunoprecipitation Assays (RIP and ChIP)**

553 RIP assays to detect mature miRNA or pri-miRNAs bound to eGFP::CARP9, HYL1, and
554 AGO1 were performed using four independent biological replicates following a reported
555 protocol with a few modifications and scaled down to 50% of the volumes (Carbonell, 2017).
556 Immunoprecipitation was performed to 4 g of tissue (flowers) using anti-GFP (AS152987,
557 dilution 1:250), antiHYL1 (AS06136, dilution 1:500) and antiAGO1 (AS09527, dilution 1:500).
558 In the case of AGO1 RIP experiments, 15-days-old UV-crosslinked plants, grown on MS agar
559 plates and treated with MG132 for 24 hours, were used as starting material. In all cases, Sure
560 Beads™ Protein-A magnetic beads (BioRad) were used for the immunoprecipitation. RNA was
561 finally extracted from the IP fraction by a regular TRIzol extraction. Associated RNA
562 quantifications were performed as described in the “RNA analysis” section of material and

563 methods. Chromatin immunoprecipitation assays of eGFP::CARP9 and DCL1 associated loci
564 were performed using antiGFP (AS152987, dilution 1:250) and antiDCL1 (AS122102, dilution
565 1:200). We first performed nuclei enriched of samples obtained from 3 g of seedlings following
566 the same protocol described above for cell fractioning assay. Extracted nuclei were then
567 resuspended in 500 µL Nuclei Lysis Buffer (50 mM Tris-HCl pH 8, 10 mM EDTA, 1 % (w/v)
568 SDS, 1 mM PMSF, 1 % (w/v) Complete Protease Inhibitors (Roche)). Chromatin was sheared
569 using a Bioruptor Pico (Diagenode; 10 cycles 30" ON, 30" OFF). After fragmentation, nuclear
570 debris was pelleted and the supernatant diluted ten-fold with ChIP Dilution Buffer (1.1 % (v/v)
571 Triton X-100, 1.2 mM EDTA, 16.7 mM Tris-HCl pH 8, 167 mM NaCl). Immunoprecipitation
572 was carried out at 4 °C overnight with 100µl of washed Sure Beads™ Protein-A magnetic beads
573 (BioRad) and the appropriate amount of antibody. After washing five times, the beads were
574 resuspended in 100 µl of TE, and 1 µl of 20 mg/ml Proteinase K added. Samples were incubated
575 at 43 °C for 1h, and the protease inactivated by incubation at 95 °C for 10 min. Samples were
576 centrifuged 1 min at maximum speed and 1.5 µl used for qPCR reactions. Negative controls
577 were performed with samples in which specific antibodies were not included. Values were
578 expressed as a % of the input signal for the same measured miRNA.

579

580 **Phylogenetic analysis** CARP9-like protein sequences of representative plant species were
581 retrieved from Phytozome (Goodstein et al., 2012) using AtCARP9 full amino acid sequence as
582 a query for BLASTP search with default parameters. Proteins sequences with low sequence
583 similarity were discarded (query coverage <30%, E-value>1.1-10). The resulting sequences
584 were aligned using the MAFFT G-INS-1 iterative method (Kato and Standley, 2013) and
585 automatically trimmed using TrimAI webserver (Capella-Gutierrez et al., 2009) with 0.9 gap
586 threshold fraction. Splicing variants were manually removed. Phylogenetic analysis was
587 performed using the Maximum likelihood (ML) method with IQTree default parameters
588 (Trifinopoulos et al., 2016) using a Shimodaira–Hasegawalike approximate likelihood ratio test.
589 The consensus tree was obtained with all compatible groups and visualized using FigTree v1.4.3
590 (<http://tree.bio.ed.ac.uk/software/figtree/>).

591

592 **CARP9 conservation analysis**

593 To test conservation of CARP9 in algae species, protein sequences of AtCARP9 and
594 *Marchantia polymorpha* CARP9 were used as a query for BLASTP search against NCBI
595 nonredundant database. Domain architecture searches were made using InterProScan (Mitchell
596 et al., 2019). Amino acid disorder score and regions were obtained from MobiDB (Piovesan et
597 al., 2018) using full protein sequences. Alignment quality was computed with Jalview
598 (Waterhouse et al., 2009) using the same alignment obtained for phylogenetic analysis. NLS

599 was predicted using cNLS Mapper (<http://nls-mapper.iab.keio.ac.jp>) with 7.0 as the cut-off
600 score.

601

602 Accession numbers

603 Sequence data from this article can be found in the GenBank data libraries under accession
604 numbers AT3G21290 (CARP9); AT1G09700 (HYL1); AT1G48410 (AGO1); (HSP90);
605 AT2G15790 (SQN); AT2G27100 (SE); AT1G01040 (DCL1); AT4G21670 (CPL1);
606 AT1G69690 (TCP15); AT2G43010 (PIF4); AT5G56010 (HSP90).

607

608 Supplemental data

609 Supplemental Figure S1. Phenotype of *carp9* mutants and rescued plants.

610 Supplemental Figure S2. Impact of CARP9 mutation on the miRNA pathway.

611 Supplemental Figure S3. Conservation of CARP9 among plants.

612 Supplemental Figure S4. CARP9 interacts with HYL1.

613 Supplemental Figure S5. CARP9 interacts with AGO1.

614 Supplemental Figure S6. CARP9 mutations impair AGO1 stability.

615 Supplemental Table S1. Differentially accumulated miRNAs as shown by small RNAseq data
616 analysis of *carp9-1* mutants.

617 Supplemental Table S2. Transgenes and plasmids.

618 Supplemental Table S3. DNA oligonucleotide primers and probes.

619

620 ACKNOWLEDGMENTS

621 We would like to thank Raquel L. Chan and Virginia Miguel for sharing the *HaHB11::C-*
622 *Citrine* construct used as a negative control for BiFC assays. CARP9 was named in honor of
623 Club Atlético River Plate from Argentina and Enzo Francescoli. This work was supported by
624 grants from ANPCyT (Agencia Nacional de Promoción Científica y Tecnológica, Argentina),
625 HFSP (Human Frontier Science Program), the Max Planck Society, ICGEB (International
626 Centre for Genetic Engineering and Biotechnology). D.A.R, J.E.M, D.A.C, A.L A and P.A.M
627 are members of CONICET; A.H.T, L.G and F.R are fellows of the same institution.

628

629 FIGURE LEGENDS

630 **Figure 1. Characterization of *carp9* mutants.** A, Gene structure of *CARP9* showing single
631 nucleotide deletion of the *carp9-1* allele and T- DNA insertion sites in *carp9-2*, *carp9-3*, *carp9-*
632 *4*, and *carp9-5*. Solid boxes and lines represent exons and introns, respectively; gray boxes
633 represent coding sequence while blue boxed shows 5'- and 3'-UTR regions. A white asterisk (*)
634 marks the position of the stop codon that results from the frameshift caused by the *carp9-1*

635 single nucleotide deletion (G2464Del). B, Phenotypic characterization of *carp9* mutants, control
636 lines (reporter and Col-0), and *carp9-1* mutants complemented by the overexpression of the
637 *CARP9* cDNA (*carp9-1*; *Pro*^{35S}:*CARP9*). 21-days-old plants, fully expanded siliques, and 40-
638 days-old plants are displayed. White bars on the right represent 1 cm. Plants were imaged
639 individually, digitally extracted, and mounted on a single black background panel to facilitate
640 comparison and observation. C, Analysis of the flowering time of control, *carp9* mutant, and
641 complemented lines grown in long-day photoperiod as measured by the number of rosette
642 leaves or the number of days to bolting. Error bars show means \pm SE ($n \geq 15$). D,
643 Bioluminescence activity, quantified by a luminometer, of 12 leave discs belonging to 20-days-
644 old *carp9-1* mutants and reporter plants. Error bars show means \pm SE ($n \geq 12$). p-values of less
645 than 0.05 (*) in a two-tailed, unpaired t-test Holm-Sidak-corrected were considered significant.
646 E, Bioluminescence activity as measured with a CCD camera, in 20-days-old *carp9-1* mutants
647 and reporter plants. Luminescence intensity is color scaled from low (blue) to high (white). Two
648 pots containing 12 plants each were imaged individually, digitally extracted, mounted in a
649 single black background panel, and displayed in the figure. E, RNA blots for detecting
650 amiRLuc. U6 was used as a loading control. F, Phenotypic features of 18-days-old *carp9*
651 mutants, control lines, and *carp9-1/capr9-2* compound heterozygous mutants. White bars on the
652 right represent 1 cm. Plants were imaged individually, digitally extracted, and mounted in a
653 single black background panel to facilitate comparison and observation.

654 **Figure 2. *CARP9* mutants present impaired miRNA activity.** A, RNA blots for detecting
655 endogenous miRNAs. U6 was used as a loading control. The relative abundance of each
656 miRNA, indicated above each band, was calculated by measuring the band intensity using
657 ImageJ and relativized to the corresponding control plant (reporter for *carp9-1* and
658 complemented plants, and Col-0 for *carp9-2*). B, MiRNA levels, as measured by RT-qPCR, in
659 mutants and control lines. Error bars show means \pm 2xSE ($n \geq 4$), p-values of less than 0.05 (*) in
660 a two-tailed, unpaired FDR-corrected t-test were considered significant. C, Mean expression
661 levels of individual miRNAs in *carp9-1* and *hyl1-2* plants relative to Col-0 plants. Horizontal
662 segments indicate the median of the expression levels. Each dot corresponds to a single miRNA
663 or collapsed miRNA family. Dark and light dots show differentially (FDR adjusted p-value <
664 0.05) and not-differentially accumulated miRNAs, respectively. D, Expression of miRNA
665 targets in control and mutant plants as measured by RT-qPCR. Error bars show means \pm 2xSE
666 ($n \geq 4$), p-values of less than 0.05 (*) in a two-tailed, unpaired t-test Holm-Sidak-corrected were
667 considered significant.

668 **Figure 3. Conservation analysis of *CARP9* across the plant kingdom.** A, On top, gene
669 structure of *CARP9* as shown in Figure 1A. On the bottom, the *CARP9* protein structure, on
670 purple is marked a putative NSL signal and its amino acid sequence. The occluding/ELL-like

671 domain is marked in red. B, Top and middle, disordered score and regions in AtCARP9 amino
672 acid sequence according to MobiDB (Piovesan et al., 2018). Bottom, amino acid alignment
673 quality of CARP9-like genes using Jalview software (Waterhouse et al., 2009), positions are
674 based on AtCARP9 full sequence. C, Phylogeny of *CARP9-like* genes in embryophytes. The
675 unrooted consensus tree was generated using the Maximum Likelihood method. Colors
676 represent different lineages of plant species, referenced in the figure. AtCARP9 is highlighted
677 with a black arrow. Supplemental Figure S3B shows the fully annotated tree. D, Confocal
678 microscopy images showing the nuclear localization of eGFP- and mCherry- tagged versions of
679 CARP9 in *N. benthamiana* transiently transformed leaves (left) and stably transformed
680 Arabidopsis plants (right). Scale bars represent 5 μ m.

681 **Figure 4. CARP9 interacts with HYL1 and mature miRNAs but not with the miRNA**
682 **processing machinery.** A, B, and C, Expression of pri-miRNA, pri-miRLuc, *HYL1* and *SE* in
683 control and mutant plants as measured by RT-qPCR. D, HYL1, and SE quantification by
684 immunoblot in samples extracted from *carp9-2* and reporter plants. The detection of ACTIN
685 was used as a loading control. E, CHIP experiment using either anti-GFP, anti-DCL1, or anti-
686 IgG antibodies in plants that express a GFP tagged version of CARP9 to detect *MIRNAs* loci
687 associated with the proteins. Primers used for the amplification are listed in the Supplemental
688 Table S3 and based on a previous report (Fang et al., 2015). ACTIN gene was used as control
689 not targeted by CARP9 nor DCL1. F, Confocal microscopy images simultaneously showing the
690 localization of CARP9 with DCL1, SE, HYL1, and CPL1 in transiently transformed *N.*
691 *benthamiana* leaves. Scale bars represent 5 μ m. G, BiFC assay in *N. benthamiana* cells showing
692 CARP9 interaction with HYL1 and SE. Negative interactions are displayed in a wider
693 magnification to show the negative interactions better. Positive interactions in a wider
694 magnification are shown in Supplemental Figure S4. Scale bars represent 5 μ m. H, Interaction
695 of CARP9 with HYL1, but not with SE, as detected by yeast two-hybrid assays. GAL4
696 activation domain (AD); GAL4 DNA binding domain (BD); -LT, medium without leucine and
697 tryptophan; -LTH, selective medium without leucine, tryptophan, and histidine. Each column
698 shows a 1:10 serial dilution. I, CARP9-HYL1 interaction detected by Co-IP assays. Leaves of
699 *A. thaliana* plants transformed with Pro35S::CARP9-eGFP were immunoprecipitated using an
700 anti-GFP antibody. Interacting HYL1 was identified using an antibody targeting the endogenous
701 protein. J and K, pri-miRNAs (J) and mature miRNAs or miRNA*s. (K) associated with
702 CARP9, or HYL1, as quantified by RIP-RTqPCR in samples extracted from plants expressing a
703 GFP tagged version of CARP9 and immunoprecipitated with either an anti-GFP, anti-HYL1 or
704 anti-IgG antibodies. Values are given as a percentage to the qPCR signal detected in the input
705 samples. (L) Precisely processed miRNA reads at all highly expressed MIRNA loci. Each dot
706 represents an individual miRNA; horizontal black bars indicate medians. miRNA levels in all

707 samples are expressed as a ratio to the precisely processed miRNAs in Col-0 plants grown at
708 23°C in LD photoperiod. In all panels involving RT-qPCR experiments, error bars show means
709 $\pm 2xSE$ ($n \geq 4$), p-values of less than 0.05 (*) or 0.01 (**) in a two-tailed, unpaired t-test were
710 considered significant.

711 **Figure 5. CARP9 interacts with AGO1 to modulate its nuclear miRNA-loading.** A, BiFC
712 assay in *Nicotiana benthamiana* cells showing CAP9 interaction with AGO1, and with HYL1 as
713 controls. The nuclear transcription factors PIF4 and TCP15 were used as negative controls and
714 displayed in a wider magnification. Scale bars represent 5 μm . B, Co-IP assays. Protein samples
715 extracted from Col-0 WT plants or plants transformed with a *35S::CARP9-eGFP* were
716 immunoprecipitated using an anti-GFP antibody, AGO1-CARP9 interaction was then detected
717 using an anti-AGO1 antibody. C, Interaction of CARP9 with HSP90 as detected by yeast two-
718 hybrid assays. GAL4 activation domain (AD); GAL4 DNA binding domain (BD); -LT,
719 medium without leucine and tryptophan; -LTH, selective medium without leucine, tryptophan,
720 and histidine. Each column shows a 1:10 serial dilution. D, Co-IP assays. Protein samples
721 extracted from Col-0 WT or *carp9-2* plants were immunoprecipitated using an anti AGO1
722 antibody, AGO1-HYL1 interaction was then detected using an anti-HYL1 antibody. AGO1 was
723 detected to test IP efficiency. E, Relative amount of mature miRNA bound to AGO1 as
724 measured by Stem-loop RT-qPCR of samples immunoprecipitated using an anti-AGO1
725 antibody. Co-IPed miRNAs were normalized to the levels of the same miRNA in the input
726 samples. For both mutants, the miRNA levels were then expressed as relative to their
727 corresponding control. Error bars show means $\pm 2xSE$ ($n=4$), p-values of less than 0.05 (*) or
728 0.01 (**) in a two-tailed, unpaired t-test were considered significant. No-antibody samples and
729 *ago1-36* mutant plants were used as negative controls for the IP experiment, not showing
730 detectable signal in the assayed conditions. F, RNA blots for detecting miRNAs in different cell
731 fractions. Quantification of U6 and tRNAs were used as a loading control and to monitor the
732 purity of the nuclear/cytoplasmic fractions. G, Quantification of the miRNA distribution
733 measured in (F). Band intensity was quantified by ImageJ and normalized by the corresponding
734 loading control. Distributions of miRNAs in the nuclear/cytoplasmic fractions were then
735 expressed as relative to Col-0 (marked as a dashed line). H, Quantification of the miRNAs
736 distribution in nucleus vs. cytoplasm fractions as measured by RT-qPCR. Each dot represents an
737 independent replicate. Significant differences were tested with an Anova test: between miRNAs
738 p-value = 0.00484; between genotypes p-value = 0.00013.

739

740 **Figure 6. AGO1 stability is compromised in CARP9 mutants.** A, AGO1 levels quantified by
741 immunoblot in samples extracted from *carp9* mutants and control plants. Levels of ACTIN were
742 measured as a loading control. B and C, Expression of pri-miRNA168 (B), and *AGO1* (C) as

743 measured by RT-qPCR. AGO1 transcript levels were measured using two sets of primers; a pair
744 amplifying the 3'-end of the transcript (Primers A) and a pair flanking the miR168 recognition
745 site in the AGO1 mRNA (Primers B). Error bars show means \pm 2xSE (n=4), p-values of less
746 than 0.05 (*) in a two-tailed, unpaired t-test were considered significant. D, AGO1 levels, as
747 measured by immunoblots, in cytoplasmic or nuclear cell fractionated samples. ACTIN and
748 Histone 3 (H3) were used to verify the purity of the fractions. E, Immunoblot quantification of
749 AGO1 levels in mutant and control plants treated with the proteasome inhibitor MG132.

750

751 **Figure 7. A model for the role of CARP9 as a scaffold in a post-pri-miRNA processing and**
752 **nuclear AGO1 loading complex.** After the processing of pri-miRNAs by DCL1, the mature
753 duplex remains associated with HYL1 and SE, which later is replaced by HEN1. CARP9 is
754 recruited to this post-processing complex by its binding to HYL1. Nuclear AGO1 is then
755 associated with the complex and HSP90 interacting with CARP9, a process leading to the
756 enhances AGO1 stability and loading of AGO1 with the mature miRNAs. Loaded AGO1 is then
757 exported to the cytosol to silence their target genes.

758

759

Parsed Citations

Achkar NP, Cambiagno DA, Manavella PA (2016) miRNA Biogenesis: A Dynamic Pathway. Trends Plant Sci 21: 1034-1044

Pubmed: [Author and Title](#)

Google Scholar: [Author Only](#) [Title Only](#) [Author and Title](#)

Achkar NP, Cho SK, Poulsen C, Arce AL, Re DA, Giudicatti AJ, Karayekov E, Ryu MY, Choi SW, Harholt J, Casal JJ, Yang SW, Manavella PA (2018) A Quick HYL1-Dependent Reactivation of MicroRNA Production Is Required for a Proper Developmental Response after Extended Periods of Light Deprivation. Dev Cell 46: 236-247 e236

Pubmed: [Author and Title](#)

Google Scholar: [Author Only](#) [Title Only](#) [Author and Title](#)

Arabidopsis Genome I (2000) Analysis of the genome sequence of the flowering plant Arabidopsis thaliana. Nature 408: 796-815

Pubmed: [Author and Title](#)

Google Scholar: [Author Only](#) [Title Only](#) [Author and Title](#)

Barauske S, Mickute M, Plotnikova A, Finke A, Venclovas C, Klimasauskas S, Vilkaitis G (2015) Functional mapping of the plant small RNA methyltransferase: HEN1 physically interacts with HYL1 and DICER-LIKE 1 proteins. Nucleic Acids Res 43: 2802-2812

Pubmed: [Author and Title](#)

Google Scholar: [Author Only](#) [Title Only](#) [Author and Title](#)

Ben Chaabane S, Liu R, Chinnusamy V, Kwon Y, Park JH, Kim SY, Zhu JK, Yang SW, Lee BH (2013) STA1, an Arabidopsis pre-mRNA processing factor 6 homolog, is a new player involved in miRNA biogenesis. Nucleic Acids Res 41: 1984-1997

Pubmed: [Author and Title](#)

Google Scholar: [Author Only](#) [Title Only](#) [Author and Title](#)

Bologna NG, Iselin R, Abriata LA, Sarazin A, Pumplin N, Jay F, Grentzinger T, Dal Peraro M, Voinnet O (2018) Nucleo-cytosolic Shuttling of ARGONAUTE1 Prompts a Revised Model of the Plant MicroRNA Pathway. Mol Cell 69: 709-719 e705

Pubmed: [Author and Title](#)

Google Scholar: [Author Only](#) [Title Only](#) [Author and Title](#)

Bologna NG, Schapire AL, Zhai J, Chorostecki U, Boisbouvier J, Meyers BC, Palatnik JF (2013) Multiple RNA recognition patterns during microRNA biogenesis in plants. Genome Res 23: 1675-1689

Pubmed: [Author and Title](#)

Google Scholar: [Author Only](#) [Title Only](#) [Author and Title](#)

Bologna NG, Voinnet O (2014) The diversity, biogenesis, and activities of endogenous silencing small RNAs in Arabidopsis. Annu Rev Plant Biol 65: 473-503

Pubmed: [Author and Title](#)

Google Scholar: [Author Only](#) [Title Only](#) [Author and Title](#)

Borges F, Parent JS, van Ex F, Wolff P, Martinez G, Kohler C, Martienssen RA (2018) Transposon-derived small RNAs triggered by miR845 mediate genome dosage response in Arabidopsis. Nat Genet 50: 186-192

Pubmed: [Author and Title](#)

Google Scholar: [Author Only](#) [Title Only](#) [Author and Title](#)

Cabello JV, Giacomelli JI, Piattoni CV, Iglesias AA, Chan RL (2016) The sunflower transcription factor HaHB11 improves yield, biomass and tolerance to flooding in transgenic Arabidopsis plants. J Biotechnol 222: 73-83

Pubmed: [Author and Title](#)

Google Scholar: [Author Only](#) [Title Only](#) [Author and Title](#)

Capella-Gutierrez S, Silla-Martinez JM, Gabaldon T (2009) trimAl: a tool for automated alignment trimming in large-scale phylogenetic analyses. Bioinformatics 25: 1972-1973

Pubmed: [Author and Title](#)

Google Scholar: [Author Only](#) [Title Only](#) [Author and Title](#)

Carbonell A (2017) Immunoprecipitation and High-Throughput Sequencing of ARGONAUTE-Bound Target RNAs from Plants. Methods Mol Biol 1640: 93-112

Pubmed: [Author and Title](#)

Google Scholar: [Author Only](#) [Title Only](#) [Author and Title](#)

Cheng CY, Krishnakumar V, Chan AP, Thibaud-Nissen F, Schobel S, Town CD (2017) Araport11: a complete reannotation of the Arabidopsis thaliana reference genome. Plant J 89: 789-804

Pubmed: [Author and Title](#)

Google Scholar: [Author Only](#) [Title Only](#) [Author and Title](#)

Cho SK, Ben Chaabane S, Shah P, Poulsen CP, Yang SW (2014) COP1 E3 ligase protects HYL1 to retain microRNA biogenesis. Nat Commun 5: 5867

Pubmed: [Author and Title](#)

Google Scholar: [Author Only](#) [Title Only](#) [Author and Title](#)

Cortese MS, Uversky VN, Dunker AK (2008) Intrinsic disorder in scaffold proteins: getting more from less. Prog Biophys Mol Biol 98: 85-106

Pubmed: [Author and Title](#)

Google Scholar: [Author Only](#) [Title Only](#) [Author and Title](#)

Cui Y, Fang X, Qi Y (2016) TRANSPORTIN1 Promotes the Association of MicroRNA with ARGONAUTE1 in Arabidopsis. Plant Cell 28: 2576-2585

Pubmed: [Author and Title](#)

Google Scholar: [Author Only](#) [Title Only](#) [Author and Title](#)

de Felippes FF, Weigel D (2010) Transient assays for the analysis of miRNA processing and function. Methods Mol Biol 592: 255-264

Pubmed: [Author and Title](#)

Google Scholar: [Author Only](#) [Title Only](#) [Author and Title](#)

Dolata J, Bajczyk M, Bielewicz D, Niedojadlo K, Niedojadlo J, Pietrykowska H, Walczak W, Szweykowska-Kulinska Z, Jarmolowski A (2016) Salt Stress Reveals a New Role for ARGONAUTE1 in miRNA Biogenesis at the Transcriptional and Posttranscriptional Levels. Plant Physiol 172: 297-312

Pubmed: [Author and Title](#)

Google Scholar: [Author Only](#) [Title Only](#) [Author and Title](#)

Dong Z, Han MH, Fedoroff N (2008) The RNA-binding proteins HYL1 and SE promote accurate in vitro processing of pri-miRNA by DCL1. Proc Natl Acad Sci U S A 105: 9970-9975

Pubmed: [Author and Title](#)

Google Scholar: [Author Only](#) [Title Only](#) [Author and Title](#)

Eamens AL, Smith NA, Curtin SJ, Wang MB, Waterhouse PM (2009) The Arabidopsis thaliana double-stranded RNA binding protein DRB1 directs guide strand selection from microRNA duplexes. RNA 15: 2219-2235

Pubmed: [Author and Title](#)

Google Scholar: [Author Only](#) [Title Only](#) [Author and Title](#)

El-Gebali S, Mistry J, Bateman A, Eddy SR, Luciani A, Potter SC, Qureshi M, Richardson LJ, Salazar GA, Smart A, Sonnhammer ELL, Hirsh L, Paladin L, Piovesan D, Tosatto SCE, Finn RD (2019) The Pfam protein families database in 2019. Nucleic Acids Res 47: D427-D432

Pubmed: [Author and Title](#)

Google Scholar: [Author Only](#) [Title Only](#) [Author and Title](#)

Fang X, Cui Y, Li Y, Qi Y (2015) Transcription and processing of primary microRNAs are coupled by Elongator complex in Arabidopsis. Nat Plants 1: 15075

Pubmed: [Author and Title](#)

Google Scholar: [Author Only](#) [Title Only](#) [Author and Title](#)

Fang X, Qi Y (2016) RNAi in Plants: An Argonaute-Centered View. Plant Cell 28: 272-285

Pubmed: [Author and Title](#)

Google Scholar: [Author Only](#) [Title Only](#) [Author and Title](#)

Fang X, Wang L, Ishikawa R, Li Y, Fiedler M, Liu F, Calder G, Rowan B, Weigel D, Li P, Dean C (2019) Arabidopsis FLL2 promotes liquid-liquid phase separation of polyadenylation complexes. Nature 569: 265-269

Pubmed: [Author and Title](#)

Google Scholar: [Author Only](#) [Title Only](#) [Author and Title](#)

Fang Y, Spector DL (2007) Identification of nuclear dicing bodies containing proteins for microRNA biogenesis in living Arabidopsis plants. Curr Biol 17: 818-823

Pubmed: [Author and Title](#)

Google Scholar: [Author Only](#) [Title Only](#) [Author and Title](#)

Ferrero LV, Viola IL, Ariel FD, Gonzalez DH (2019) Class I TCP Transcription Factors Target the Gibberellin Biosynthesis Gene GA20ox1 and the Growth-Promoting Genes HBI1 and PRE6 during Thermomorphogenic Growth in Arabidopsis. Plant Cell Physiol 60: 1633-1645

Pubmed: [Author and Title](#)

Google Scholar: [Author Only](#) [Title Only](#) [Author and Title](#)

Francisco-Mangilet AG, Karlsson P, Kim MH, Eo HJ, Oh SA, Kim JH, Kulcheski FR, Park SK, Manavella PA (2015) THO2, a core member of the THO/TREX complex, is required for microRNA production in Arabidopsis. Plant J 82: 1018-1029

Pubmed: [Author and Title](#)

Google Scholar: [Author Only](#) [Title Only](#) [Author and Title](#)

Goodstein DM, Shu S, Howson R, Neupane R, Hayes RD, Fazo J, Mitros T, Dirks W, Hellsten U, Putnam N, Rokhsar DS (2012) Phytosome: a comparative platform for green plant genomics. Nucleic Acids Res 40: D1178-1186

Pubmed: [Author and Title](#)

Google Scholar: [Author Only](#) [Title Only](#) [Author and Title](#)

Jarvelin AI, Noerenberg M, Davis I, Castello A (2016) The new (dis)order in RNA regulation. Cell Commun Signal 14: 9

Pubmed: [Author and Title](#)

Google Scholar: [Author Only](#) [Title Only](#) [Author and Title](#)

Karlsson P, Christie MD, Seymour DK, Wang H, Wang X, Haggmann J, Kulcheski F, Manavella PA (2015) KH domain protein RCF3 is a tissue-biased regulator of the plant miRNA biogenesis cofactor HYL1. Proc Natl Acad Sci U S A 112: 14096-14101

Pubmed: [Author and Title](#)

Google Scholar: [Author Only](#) [Title Only](#) [Author and Title](#)

Katoh K, Standley DM (2013) MAFFT multiple sequence alignment software version 7: improvements in performance and usability. Mol Biol Evol 30: 772-780

Pubmed: [Author and Title](#)

Google Scholar: [Author Only](#) [Title Only](#) [Author and Title](#)

Kramer MF (2011) Stem-loop RT-qPCR for miRNAs. Curr Protoc Mol Biol Chapter 15: Unit 15 10

Pubmed: [Author and Title](#)

Google Scholar: [Author Only](#) [Title Only](#) [Author and Title](#)

Kurihara Y, Watanabe Y (2004) Arabidopsis micro-RNA biogenesis through Dicer-like 1 protein functions. Proc Natl Acad Sci U S A 101: 12753-12758

Pubmed: [Author and Title](#)

Google Scholar: [Author Only](#) [Title Only](#) [Author and Title](#)

Li J, Yang Z, Yu B, Liu J, Chen X (2005) Methylation protects miRNAs and siRNAs from a 3'-end uridylation activity in Arabidopsis. Curr Biol 15: 1501-1507

Pubmed: [Author and Title](#)

Google Scholar: [Author Only](#) [Title Only](#) [Author and Title](#)

Li S, Castillo-Gonzalez C, Yu B, Zhang X (2017) The functions of plant small RNAs in development and in stress responses. Plant J 90: 654-670

Pubmed: [Author and Title](#)

Google Scholar: [Author Only](#) [Title Only](#) [Author and Title](#)

Li Y, Fanning AS, Anderson JM, Lavie A (2005) Structure of the conserved cytoplasmic C-terminal domain of occludin: identification of the ZO-1 binding surface. J Mol Biol 352: 151-164

Pubmed: [Author and Title](#)

Google Scholar: [Author Only](#) [Title Only](#) [Author and Title](#)

Liu C, Xin Y, Xu L, Cai Z, Xue Y, Liu Y, Xie D, Liu Y, Qi Y (2018) Arabidopsis ARGONAUTE 1 Binds Chromatin to Promote Gene Transcription in Response to Hormones and Stresses. Dev Cell 44: 348-361 e347

Pubmed: [Author and Title](#)

Google Scholar: [Author Only](#) [Title Only](#) [Author and Title](#)

Lobbes D, Rallapalli G, Schmidt DD, Martin C, Clarke J (2006) SERRATE: a new player on the plant microRNA scene. EMBO Rep 7: 1052-1058

Pubmed: [Author and Title](#)

Google Scholar: [Author Only](#) [Title Only](#) [Author and Title](#)

Ma Z, Castillo-Gonzalez C, Wang Z, Sun D, Hu X, Shen X, Potok ME, Zhang X (2018) Arabidopsis Serrate Coordinates Histone Methyltransferases ATXR5/6 and RNA Processing Factor RDR6 to Regulate Transposon Expression. Dev Cell 45: 769-784 e766

Pubmed: [Author and Title](#)

Google Scholar: [Author Only](#) [Title Only](#) [Author and Title](#)

Manavella PA, Haggmann J, Ott F, Laubinger S, Franz M, Macek B, Weigel D (2012) Fast-forward genetics identifies plant CPL phosphatases as regulators of miRNA processing factor HYL1. Cell 151: 859-870

Pubmed: [Author and Title](#)

Google Scholar: [Author Only](#) [Title Only](#) [Author and Title](#)

Manavella PA, Yang SW, Palatnik J (2019) Keep calm and carry on: miRNA biogenesis under stress. Plant J

Pubmed: [Author and Title](#)

Google Scholar: [Author Only](#) [Title Only](#) [Author and Title](#)

Mitchell AL, Attwood TK, Babbitt PC, Blum M, Bork P, Bridge A, Brown SD, Chang HY, El-Gebali S, Fraser MI, Gough J, Haft DR, Huang H, Letunic I, Lopez R, Luciani A, Madeira F, Marchler-Bauer A, Mi H, Natale DA, Necci M, Nuka G, Orengo C, Pandurangan AP, Paysan-Lafosse T, Pesseat S, Potter SC, Qureshi MA, Rawlings ND, Redaschi N, Richardson LJ, Rivoire C, Salazar GA, Sangrador-Vegas A, Sigrist CJA, Sillitoe I, Sutton GG, Thanki N, Thomas PD, Tosatto SCE, Yong SY, Finn RD (2019) InterPro in 2019: improving coverage, classification and access to protein sequence annotations. Nucleic Acids Res 47: D351-D360

Pubmed: [Author and Title](#)

Google Scholar: [Author Only](#) [Title Only](#) [Author and Title](#)

Moro B, Chorostecki U, Arikat S, Suarez IP, Hobartner C, Rasia M, Meyers BC, Palatnik JF (2018) Efficiency and precision of microRNA biogenesis modes in plants. Nucleic Acids Res 46: 10709-10723

Pubmed: [Author and Title](#)

Google Scholar: [Author Only](#) [Title Only](#) [Author and Title](#)

Park MY, Wu G, Gonzalez-Sulser A, Vaucheret H, Poethig RS (2005) Nuclear processing and export of microRNAs in Arabidopsis. Proc Natl Acad Sci U S A 102: 3691-3696

Pubmed: [Author and Title](#)

Google Scholar: [Author Only](#) [Title Only](#) [Author and Title](#)

Piovesan D, Tabaro F, Paladin L, Necci M, Micetic I, Camilloni C, Davey N, Dosztanyi Z, Meszaros B, Monzon AM, Parisi G, Schad E, Sormanni P, Tompa P, Vendruscolo M, Vranken WF, Tosatto SCE (2018) MolDB 3.0: more annotations for intrinsic disorder, and more

conformational diversity and interactions in proteins. Nucleic Acids Res 46: D471-D476

Pubmed: [Author and Title](#)

Google Scholar: [Author Only](#) [Title Only](#) [Author and Title](#)

Potenza E, Di Domenico T, Walsh I, Tosatto SC (2015) MobiDB 2.0: an improved database of intrinsically disordered and mobile proteins. Nucleic Acids Res 43: D315-320

Pubmed: [Author and Title](#)

Google Scholar: [Author Only](#) [Title Only](#) [Author and Title](#)

Rajagopalan R, Vaucheret H, Trejo J, Bartel DP (2006) A diverse and evolutionarily fluid set of microRNAs in Arabidopsis thaliana. Genes Dev 20: 3407-3425

Pubmed: [Author and Title](#)

Google Scholar: [Author Only](#) [Title Only](#) [Author and Title](#)

Re DA, Cambiagno DA, Arce AL, Tomassi AH, Giustozzi M, Casati P, Ariel FD, Manavella PA (2020) CURLY LEAF Regulates MicroRNA Activity by Controlling ARGONAUTE 1 Degradation in Plants. Mol Plant 13: 72-87

Pubmed: [Author and Title](#)

Google Scholar: [Author Only](#) [Title Only](#) [Author and Title](#)

Re DA, Lang PLM, Yones C, Arce AL, Stegmayer G, Milone D, Manavella PA (2019) Alternative use of miRNA-biogenesis co-factors in plants at low temperatures. Development 146

Pubmed: [Author and Title](#)

Google Scholar: [Author Only](#) [Title Only](#) [Author and Title](#)

Rogers K, Chen X (2012) microRNA biogenesis and turnover in plants. Cold Spring Harb Symp Quant Biol 77: 183-194

Pubmed: [Author and Title](#)

Google Scholar: [Author Only](#) [Title Only](#) [Author and Title](#)

Schalk C, Cognat V, Graindorge S, Vincent T, Voinnet O, Molinier J (2017) Small RNA-mediated repair of UV-induced DNA lesions by the DNA DAMAGE-BINDING PROTEIN 2 and ARGONAUTE 1. Proc Natl Acad Sci U S A 114: E2965-E2974

Pubmed: [Author and Title](#)

Google Scholar: [Author Only](#) [Title Only](#) [Author and Title](#)

Shilatfard A, Lane WS, Jackson KW, Conaway RC, Conaway JW (1996) An RNA polymerase II elongation factor encoded by the human ELL gene. Science 271: 1873-1876

Pubmed: [Author and Title](#)

Google Scholar: [Author Only](#) [Title Only](#) [Author and Title](#)

Speth C, Szabo EX, Martinho C, Collani S, Zur Oven-Krockhaus S, Richter S, Droste-Borel I, Macek B, Stierhof YD, Schmid M, Liu C, Laubinger S (2018) Arabidopsis RNA processing factor SERRATE regulates the transcription of intronless genes. Elife 7

Pubmed: [Author and Title](#)

Google Scholar: [Author Only](#) [Title Only](#) [Author and Title](#)

Sun H, Schneeberger K (2015) SHOREmap v3.0: fast and accurate identification of causal mutations from forward genetic screens. Methods Mol Biol 1284: 381-395

Pubmed: [Author and Title](#)

Google Scholar: [Author Only](#) [Title Only](#) [Author and Title](#)

Tomassi AH, Gagliardi D, Cambiagno DA, Manavella PA (2017) Nonradioactive Detection of Small RNAs Using Digoxigenin-Labeled Probes. Methods Mol Biol 1640: 199-210

Pubmed: [Author and Title](#)

Google Scholar: [Author Only](#) [Title Only](#) [Author and Title](#)

Tompa P, Kovacs D (2010) Intrinsically disordered chaperones in plants and animals. Biochem Cell Biol 88: 167-174

Pubmed: [Author and Title](#)

Google Scholar: [Author Only](#) [Title Only](#) [Author and Title](#)

Tompa P, Schad E, Tantos A, Kalmar L (2015) Intrinsically disordered proteins: emerging interaction specialists. Curr Opin Struct Biol 35: 49-59

Pubmed: [Author and Title](#)

Google Scholar: [Author Only](#) [Title Only](#) [Author and Title](#)

Trifinopoulos J, Nguyen LT, von Haeseler A, Minh BQ (2016) W-IQ-TREE: a fast online phylogenetic tool for maximum likelihood analysis. Nucleic Acids Res 44: W232-235

Pubmed: [Author and Title](#)

Google Scholar: [Author Only](#) [Title Only](#) [Author and Title](#)

Uversky VN, Kuznetsova IM, Turoverov KK, Zaslavsky B (2015) Intrinsically disordered proteins as crucial constituents of cellular aqueous two phase systems and coacervates. FEBS Lett 589: 15-22

Pubmed: [Author and Title](#)

Google Scholar: [Author Only](#) [Title Only](#) [Author and Title](#)

Van Itallie CM, Anderson JM (2018) Phosphorylation of tight junction transmembrane proteins: Many sites, much to do. Tissue Barriers 6: e1382671

Pubmed: [Author and Title](#)

Google Scholar: [Author Only](#) [Title Only](#) [Author and Title](#)

Varadi M, Zsolyomi F, Guharoy M, Tompa P (2015) Functional Advantages of Conserved Intrinsic Disorder in RNA-Binding Proteins. PLoS One 10: e0139731

Pubmed: [Author and Title](#)

Google Scholar: [Author Only](#) [Title Only](#) [Author and Title](#)

Vaucheret H, Vazquez F, Crete P, Bartel DP (2004) The action of ARGONAUTE1 in the miRNA pathway and its regulation by the miRNA pathway are crucial for plant development. Genes Dev 18: 1187-1197

Pubmed: [Author and Title](#)

Google Scholar: [Author Only](#) [Title Only](#) [Author and Title](#)

Wang W, Ye R, Xin Y, Fang X, Li C, Shi H, Zhou X, Qi Y (2011) An importin beta protein negatively regulates MicroRNA activity in Arabidopsis. Plant Cell 23: 3565-3576

Pubmed: [Author and Title](#)

Google Scholar: [Author Only](#) [Title Only](#) [Author and Title](#)

Waterhouse AM, Procter JB, Martin DM, Clamp M, Barton GJ (2009) Jalview Version 2--a multiple sequence alignment editor and analysis workbench. Bioinformatics 25: 1189-1191

Pubmed: [Author and Title](#)

Google Scholar: [Author Only](#) [Title Only](#) [Author and Title](#)

Wei W, Ba Z, Gao M, Wu Y, Ma Y, Amiard S, White CI, Rendtlew Danielsen JM, Yang YG, Qi Y (2012) A role for small RNAs in DNA double-strand break repair. Cell 149: 101-112

Pubmed: [Author and Title](#)

Google Scholar: [Author Only](#) [Title Only](#) [Author and Title](#)

Yang SW, Chen HY, Yang J, Machida S, Chua NH, Yuan YA (2010) Structure of Arabidopsis HYPONASTIC LEAVES1 and its molecular implications for miRNA processing. Structure 18: 594-605

Pubmed: [Author and Title](#)

Google Scholar: [Author Only](#) [Title Only](#) [Author and Title](#)

Zhu H, Zhou Y, Castillo-Gonzalez C, Lu A, Ge C, Zhao YT, Duan L, Li Z, Axtell MJ, Wang XJ, Zhang X (2013) Bidirectional processing of pri-miRNAs with branched terminal loops by Arabidopsis Dicer-like1. Nat Struct Mol Biol 20: 1106-1115

Pubmed: [Author and Title](#)

Google Scholar: [Author Only](#) [Title Only](#) [Author and Title](#)